THE PENNSYLVANIA STATE UNIVERSITY
SCHREYER HONORS COLLEGE

DEPARTMENT OF BIOENGINEERING

THE EFFECTS OF MULTIPLE KINESIN MOTORS ON CARGO TRANSPORT VELOCITY

NICHOLAS ROBERT BIZZARO
Fall 2010

A thesis
submitted in partial fulfillment
of the requirements
for a baccalaureate degree
in Bioengineering
with honors in Bioengineering

Reviewed and approved* by the following:

William O. Hancock
Associate Professor of Bioengineering
Thesis Supervisor & Honors Adviser

Peter J. Butler
Associate Professor of Bioengineering
Faculty Reader

Margaret J. Slattery
Assistant Professor of Bioengineering
Faculty Reader

* Signatures are on file in the Schreyer Honors College.

ABSTRACT

The function of kinesin molecular motors is to transport cargo within a cell along microtubules. Observation of *in vivo* cargo transport has led researchers to believe that molecular motors often work together to carry cargo within a cell. When multiple motors attach to cargo they can cooperatively regulate cargo's transport properties. The cargo transport velocity that results is related to the properties of the assemblies of each type of motor that is bound to the cargo.

This thesis aims to evaluate current mathematical models used to predict the resultant cargo velocity of cooperative transport with multiple kinesin motors and understand the best conditions in which to apply them. Models have been proposed that relate basic transport properties of different kinesin motors and their respective mole fractions to predict a resultant velocity based on these measurements. The specific properties of the different motors are expected to have a significant impact on the movement of the cargo, depending on which motors are mixed together.

Cargo transport using two different kinesin motors can be evaluated experimentally using microtubule gliding motility assays. This experiment permits direct observation of *in vitro* cargo transport of fluorescent microtubules by kinesin motors. The velocity data from the motility assay helps characterize the cooperative movement of cargo that is transported by more than one type of kinesin motor.

TABLE OF CONTENTS

LIST OF FIGURES

ACKNOWLEDGEMENTS

I would like to thank Dr. William Hancock for his knowledge, advisement, and patience over the years.

I would like to dedicate this thesis to my family, all of whom have provided me with unlimited support.

Chapter 1: Introduction

Kinesin motor proteins are a family of proteins whose function it is to transport cargo within eukaryotic cells using ATP hydrolysis to generate force. This cargo can include organelles, mRNA, intermediate filaments, and signaling molecules (Yildiz, 2004). Kinesins transport this cargo within eukaryotic cells by walking along microtubules that make a highway of sorts within the cell. This process allows for cargo to be moved within the cell more efficiently than by passive diffusion alone.

In order to fully understand how these molecular motor proteins work it is important to understand the structure and function of microtubules within the cell. Microtubules are the largest of the three structural elements of the cytoskeleton of eukaryotic cells and are built of alternating subunits of alpha and beta tubulin, a small protein (Li, 2002). These cylinders are approximately twenty-five nanometers in diameter and can vary in length from hundreds of nanometers to tens of micrometers (Tilney, 1973).

The alpha and beta subunits first bind alternately to each other, end to end, to form a protofilament with a polarity (alpha tubulin representing the plus-end, beta tubulin representing the minus-end). Thirteen of these protofilaments will line up in parallel to form a hollow, cylindrical microtubule with the same polarity as the protofilaments. The polarity is noted because kinesin only moves toward the plus-end of microtubules which is usually in the direction from the center to the periphery of the cell. Microtubules can be polymerized from tubulin and stabilized by adding taxol to the solution (Schiff, 1979).

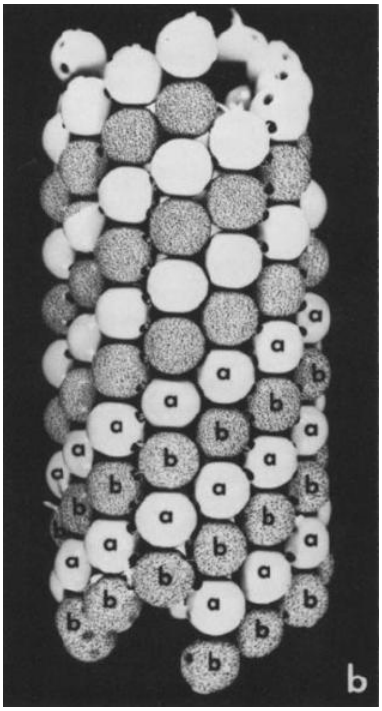

Figure 1-1: Microtubule composed of a ring of thirteen polar protofilaments of alternating subunits of alpha and beta tubulin (Tilney, 1973)

Kinesin motors are dimers with a quaternary structure composed of two "heavy" and two "light" polypeptide chains (Bloom, 1988). Each monomer has four major sections: the motor domain (head), a flexible neck linker, an alpha helix stalk, and a cargo binding domain (tail).

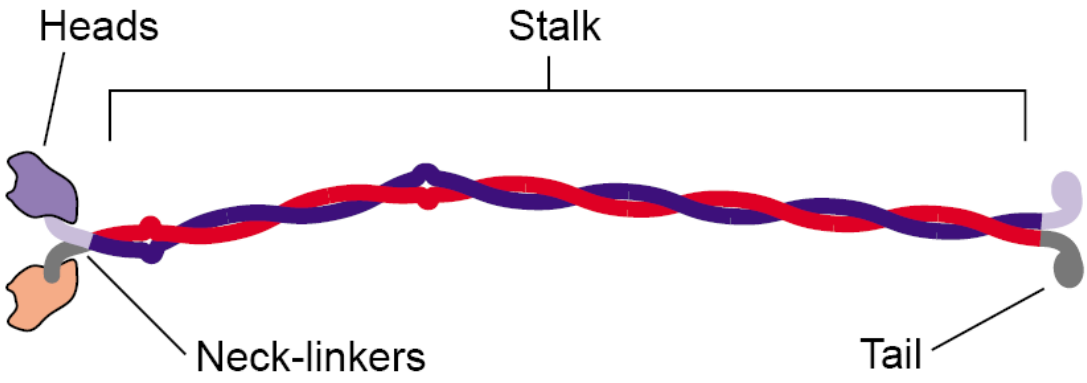

Figure 1-2: Basic structure of a dimeric kinesin motor (Asbury, 2005)

The motor domain is a ~340 amino acid long chain that hydrolyzes ATP and produces motion along the microtubule. Using X-ray crystallography the globular structure of the motor domain has been determined to be an eight-stranded beta sheet that has three alpha helices and a small three-stranded beta sheet surrounding it on both sides (Kull, 1996). The head has two binding sites, one on the front for ATP binding and another on its back for microtubule binding (Mandelkow, 1999).

Connected to the motor domain is a highly conserved, flexible ~15 amino acid chain dubbed the "neck linker." The neck linker has been shown to be critical in the processivity of the kinesin motors. Processivity is defined as the number of steps that a molecular motor walks along a microtubule before both heads dissociate and the motor is no longer bound. Experiments involving mutating the composition and structure of the neck linker have resulted in a 200-500 fold decrease in the velocity of microtubules even though the amount of ATP hydrolyzed by the motor was only three times less than a wild-type kinesin (Case, 2000). The neck linker region may aid in the synchronization of the two motor heads in kinesin dimers as they walk along the microtubule through the conformational changes that take place in the structure of the neck linkers while in the presence of different nucleotides (Asenjo, 2006).

The third piece of the heavy chain, the stalk, is an alpha helical structure that is attached to the motor domain by the neck linker. This alpha helix binds with the alpha helix of another kinesin monomer to form a coiled coil alpha helical stalk in dimerized kinesin (Hirokawa, 1989). This coiled coil is what keeps the two monomers connected as they walk along the microtubule.

At the end of the heavy chain is a ~60 amino acid fan-shaped globular tail that, in conjunction with the light chain, binds to the cargo being transported by the motor (Hirokawa, 1989). For in vitro motility the light chain is not needed for processivity and is often not included in kinesin constructs (Yang, 1990). In addition to being the binding domain for the cargo, the tail

can regulate the actions of the motor domain depending on its conformation. When in its native unbound state, the tail is much closer to the head, limiting ATPase activity. In the presence of microtubules, the ATPase rate of kinesin motors with cargo bound to their tails is three- to seven-fold higher than motors without bound cargo. Additionally, the ATPase rate of tail-less kinesin motors is similar to that of kinesin motors with tail-bound cargo (Coy, 1999), further suggesting that the native conformation of the tail inhibits ATPase activity.

The cargo is moved along the microtubule through the coordinated actions of the two motor domains of the kinesin dimer. Kinesin can take hundreds of 8 nanometer steps along a microtubule, hydrolyzing one molecule of ATP each step, before completely dissociating (Schnitzer, 1997). This high level of processivity suggests that that one of the two motor heads is always bound to the microtubule while the motor is moving along it (Rosenfeld, 2003). The two motor heads must be able to communicate to one another their respective enzymatic states in order to coordinate movement (Toprak, 2009).

The coordinated stepping of the kinesin motor domains has been studied and modeled. The "hand-over-hand" model proposes that kinesin motor heads take alternating steps along the microtubule. This stepping resembles a walking motion, much like a biped, with the front head bound in place while the rear head steps forward to bind in front of it. The conformational changes in the structure of the kinesin molecule that make the stepping motion are the result of the binding and hydrolysis of ATP resulting in a cycle that couples chemical and mechanical changes.

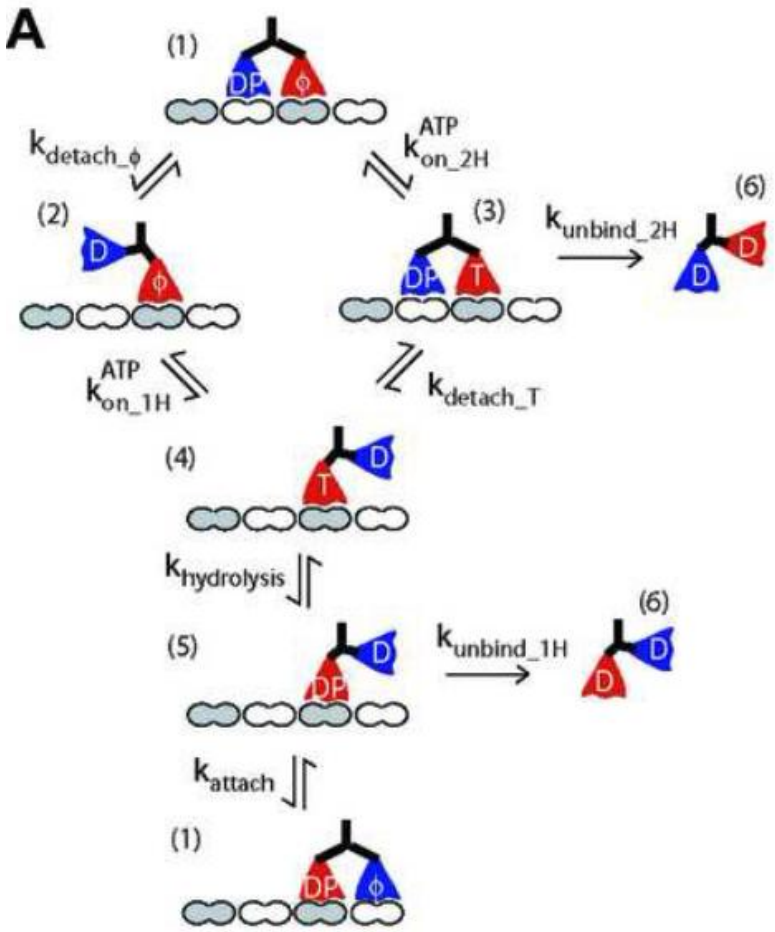

Figure 1-3: Modeling the kinesin chemomechanical cycle (Shastry, 2010)

The kinesin dimer begins the cycle with both heads bound to the microtubule. The front head is in a nucleotide free state which the rear head is bound to a molecule of ADP and inorganic phosphorous in State 1. There are two possible conformations that the kinesin molecule can enter from this state. If an ATP molecule binds before the rear head detaches due to strain, then the motor will enter State 3 at which point it can hydrolyze the ATP and dissociate from the microtubule completely, State 6, or the rear ADP bound head detaches and the motor enters State 4. If the rear head detaches due to strain before the front head binds ATP, the molecule enters the nucleotide free, single head bound State 2 after which the bound head binds

an ATP molecule, State 4. Once in State 4, the single bound motor head will hydrolyze its ATP and the motor will dissociate completely, State 6, or the unbound head will rebind at the next available microtubule binding site and reenter state 1. At this point the motor is in the same conformation it stated in with the motor heads in opposite positions. This cycle repeats with each head taking alternating steps of 16 nm and 0 nm resulting in an 8 nm step forward of the center of mass of the kinesin motor per ATP molecule hydrolyzed. Understanding how the "hand-over-hand" model describes the processivity of kinesin is important in understanding how kinesin can work cooperatively to carry cargo.

Kinesin molecules have been determined to have two binding conformations that control the stepping cycle of the motor, single and double-headed binding. Experiments have shown that the nucleotide environment affects which binding state the kinesin molecule is in. Single head binding is observed when the motor is in an environment with either no nucleotides or a mix of ADP and AMP-PNP. In the presence of only AMP-PNP, kinesin molecules are observed to be in a state with both heads bound to the microtubule (Kawaguchi, 2001).

Single molecule experiments using beads and optical tweezers have determined that kinesin motor heads are more tightly bound to the microtubule when in the nucleotide free or ATP bound state as compared to when they are bound to ADP (Uemura, 2002). The observed differences in binding forces and conformations between the nucleotide states are consistent with the stepping mechanics of the hand-over-hand model.

Comparing mutant kinesin with only one motor domain with standard two-headed kinesin molecules reveals much about the chemomechanical cycle of kinesin. It takes four to six single headed motors to move a microtubule when it only takes a single dimeric kinesin molecule to do the same (Hancock, 1998). The ATPase rate and detachment rate in the ADP-Pi state for single headed kinesin are also found to be at least one order of magnitude lower than double

headed kinesin, suggesting that the binding of the second motor head accelerates the unbinding of the first motor head (Hancock, 1999).

Neck linkers are thought to cause internal loads on the motor heads that affect their nucleotide binding (Schief, 2004) and accordingly, their processivity. Experiments have shown that changing the length of the neck linker can result in a change in the processivity of the motor. When the 14 amino acid neck linker of the optimally processive Kinesin-1 motor was increased by 1, 2, and 3 amino acid residues the communication between the two motor heads became increasingly diminished and processivity decreased. Conversely, when the 17 amino acid neck linker of the less processive Kinesin-2 motor was shortened it became more processive, due to an increase in the tension and mechanical communication between the motor heads (Shastry, 2010).

The affinity that a motor head has for binding a molecule of ADP, consequently resulting in a weak bond to the microtubule, is dependent upon the direction of the load placed on it. Kinesin motor heads that have a plus-ended load (rear head) applied to them have higher affinities for ADP than do motor heads with a minus-ended load (front head) (Uemura, 2003).

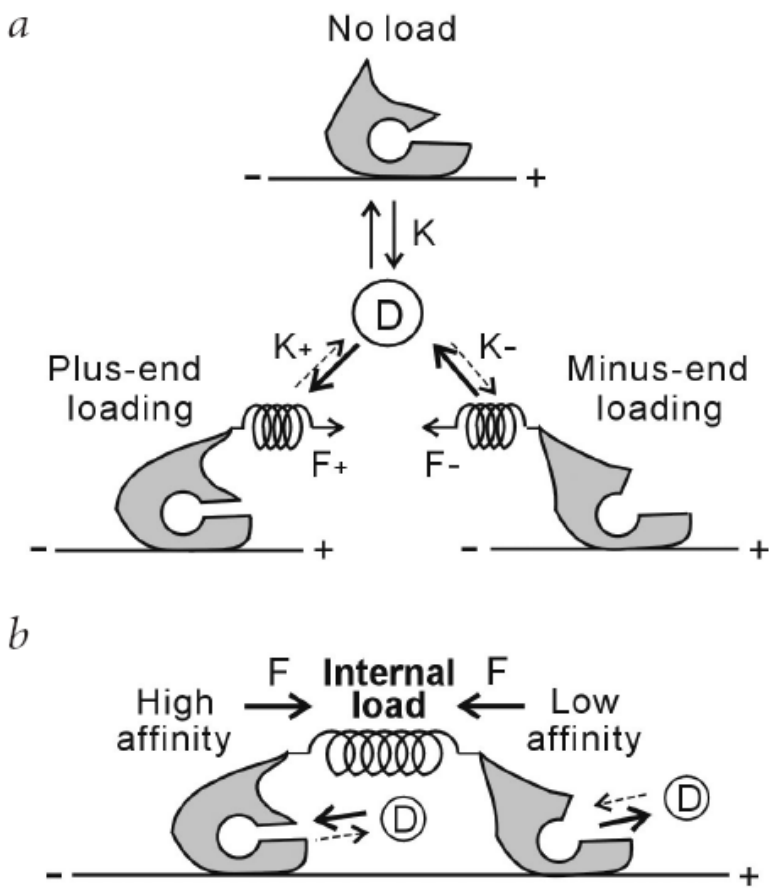

Figure 1-4: Illustration depicting the effect of internal load caused by the neck linker on the binding affinity of ADP (Uemura, 2003).

The unbinding force of kinesin motors is not symmetrical depending on the direction of the force applied. It has been experimentally determined that the dissociation force of plus-end directed forces are only 45% of the dissociation force of minus-end directed forces (Uemura, 2002). This dissociation force asymmetry is consistent with the data that shows that the rear motor has a greater affinity for ADP and thus is more likely to dissociate than the front gated motor. The rear head's higher affinity for ADP is important to kinesin motors walking forward along a microtubule.

The direction dependent asymmetry of motor dissociation forces can play an important role in the velocity of cargo transport by multiple motors. In a motility assay using a combination of fast and slow motors, the slow motors will have a plus-ended force applied to them by the fast motors and the slow motors will have a minus-ended force applied (Larson, 2009). The asymmetry of the dissociation force may result in the fast motors accelerating the slow motors' dissociation, providing the binding rates and stall forces (force that results in a zero velocity when an external load is applied) are the same.

Since the discovery of the kinesin family of molecular motors, many experiments have been performed to determine kinesin's stepping mechanics, speed, force generation, and run length (distance moved along microtubule at one time). Most of the experiments performed have used single molecule techniques without giving much consideration to how multiple kinesin motors interact cooperatively. Kinesin motors, as well as other cytoskeleton motors, have been observed working together to transport cargo within a cell using electron microscopy (Ashkin, 1990). In vivo experiments on the velocity and force generation of molecular motors support these observations (Levi, 2006; Kural, 2005).

Molecular motors commonly work cooperatively to overcome some disadvantages that single motors may face when transporting cargo. As expected, multiple motors moving in the same direction along the microtubule has been determined to exert a greater force on cargo than a single motor can by itself (Vershinin, 2007). This extra force permits cargo with a high drag coefficient to be transported throughout the cell with greater speed than with a single motor, though the force that is generated by multiple motors is not thought to scale linearly with the single motor force due to asynchronous motor stepping causing negative interference between motors.

Observed instantaneous changes in vesicular cargo velocity (Rogers, 2009) and the velocity of some microtubule segments with respect to the end of the microtubule (Larson, 2009) suggest that kinesin stepping is not necessarily synchronized. This is reasonable considering that the time that kinesin takes to step is much shorter than the time it spends waiting to step (Bieling, 2008). This lack of coordination results in internal forces being created along the microtubule that are distributed across the motors and increase their unbinding rates. Unbinding rates increase exponentially with increasing internal forces suggesting that the dominance of one type of motor will result in an unbinding cascade for the other motor type (Müller, 2008). This can result in fast motors overpowering slow motors even at small mole fractions leading to rapid changes in velocity for the cargo as the mole fraction of fast motors is increased.

Longer run lengths have also been observed when multiple motors are attached to the cargo at the same time. This is a result of there being a smaller probability of all of the kinesin motors being unbound from the microtubule at any given time, thus keeping it in motion for a longer distance. The run length is also increased by multiple motors because they can step from one microtubule to another filament as opposed to being limited to a run length equal to the length of a single microtubule as single motors are (Kuznetsov, 1992). The coordination of multiple molecular motors attached to a single cargo, whether they are in the same family or not, can be used for the purpose of regulating the movement of the cargo within the cell (Mallik, 2004).

Since kinesin motors cannot be directly observed when they are walking, experiments have been designed to help visualize their effects on cargo transport. In microtubule gliding assays, kinesin molecules are immobilized by binding their tails to a glass microscope slide, leaving the motor domains facing up. Casein is generally used to coat the surface of the glass before binding the motors to be preserve kinesin processivity (Ozeki, 2009). Microtubules bind

to and are moved by the motors. If the tubulin is labeled with rhodamine fluorophores before it is polymerized into microtubules, the microtubules can be visualized using fluorescent microscopy to observe and track microtubule movement along the motors in order to determine the velocity at which it is being carried.

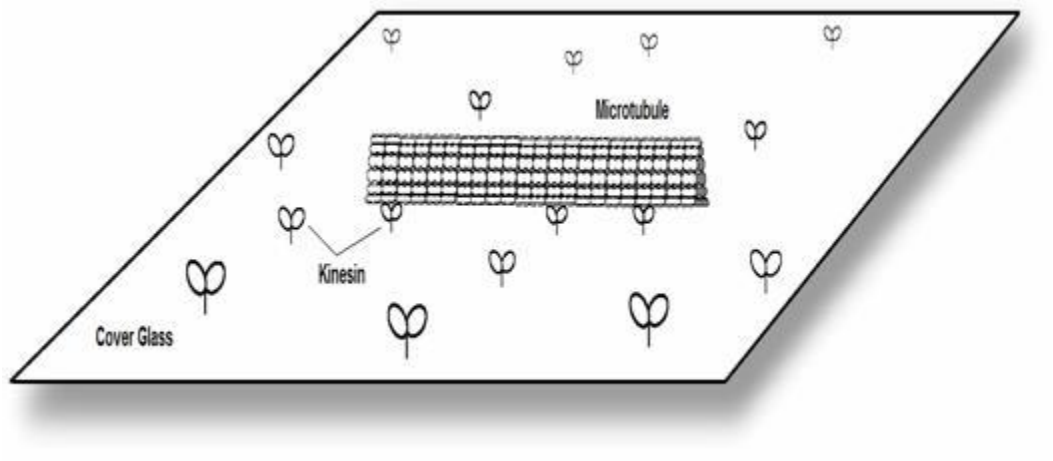

Figure 1-5: Illustration of a microtubule motility gliding assay

Microtubule motility gliding assays are used in this thesis to determine the effect that different kinesin motor combinations and mixtures have on the velocity of cargo. Motor density on the surface is kept constant in order to ensure the same number of motors bind to the microtubule in each experiment, but the concentration of the two types of motors vary. In this way the effect that each motor has on the velocity of the microtubule as a fraction of the total number of motors can be observed. Performing gliding assays with the same motor combinations and fractions at very high and very low motor dilutions provide data on whether or not the coordination of the motors is consistent and scalable.

There are several models that are generally used to describe the speed of cargo transport depending on the mole ratios of the kinesin motors that are present. Pan *et al.* has suggested two models using a combination of homodimeric OSM-3 and heterotrimeric Kinesin-2, two Kinesin-2 family motors that appear to be regulated in cooperative intraflagellar transport. In one model,

dubbed the "alternating action model," Figure 1-6, the different kinesin motors take turns stepping along the microtubule. Each type of motor takes a number of steps in proportion to its mole ratio resulting in an intermediate speed of cargo transport.

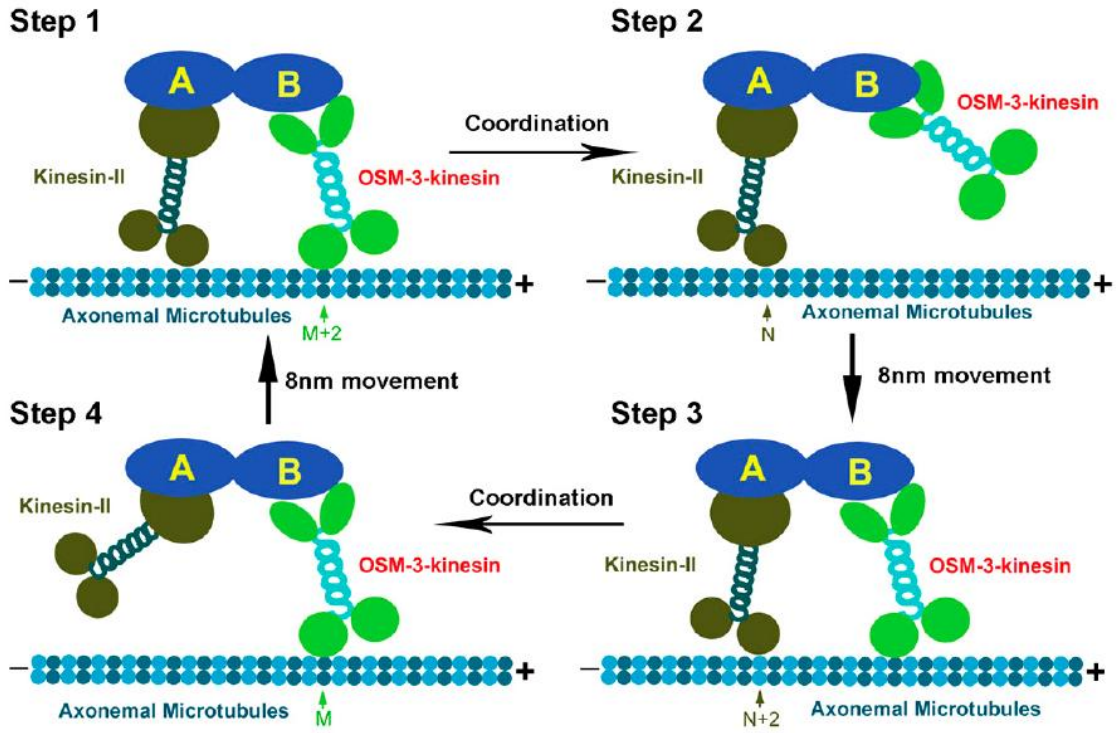

Figure 1-6: Illustration of the alternating action model (Pan et al. 2006)

Another model, the "mechanical competition model," as seen in Figure 1-7, assumes that both motors are always stepping along the microtubule and exerting forces on each other. In this model, the fast motors are pulling the slow motors forward while the slow motors are holding the fast motors back producing an intermediate net force on the microtubule that transports it with an intermediate speed.

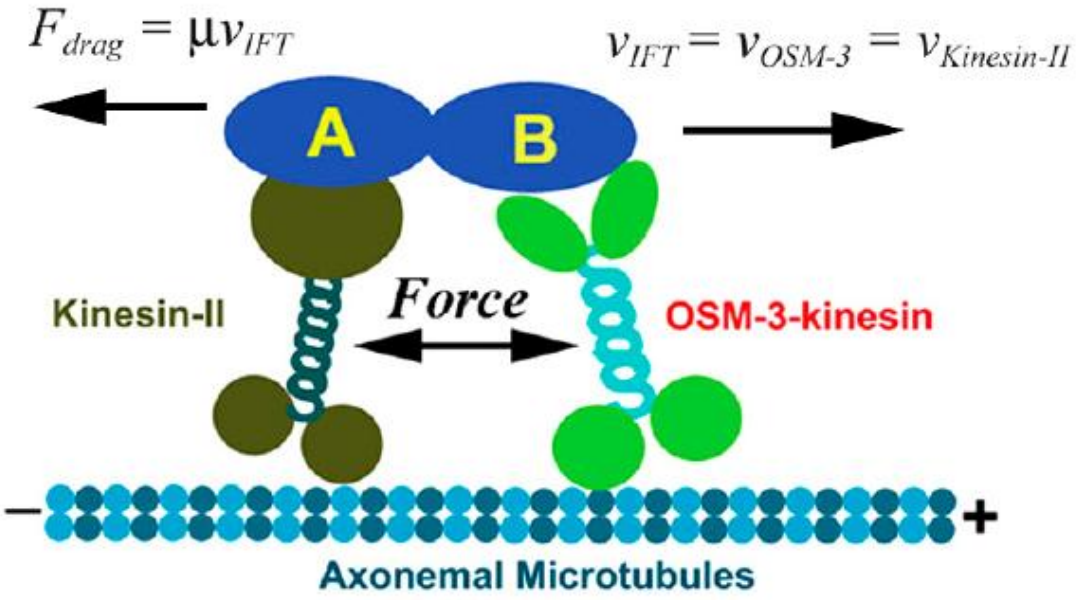

Figure 1-7: Illustration of the mechanical competition model (Pan et al. 2006)

The alternating action model predicts that a mixture of motors with different stepping speeds will cooperatively carry cargo at a speed that is between the two speeds of the motors and is related to their respective mole ratios. This stepping occurs sequentially, meaning that only one type of motor is stepping along the microtubule at any given time, transporting it at the speed that the motor moves at by itself. The binding and unbinding rates and velocity of each motor are assumed to be unchanged from their independently measured single motor values. The intermediate speed of cargo transport that results is calculated by simply dividing the number of steps taken by each motor (with respect to their mole fraction) by the length of time that they were stepping, assuming that each step taken is 8 nanometers.

If there are a two types of kinesin motors, *A* and *B*, taking 8 nanometer steps and the number of motors bound to the cargo are *M and N*, respectively, then the total run length, in nanometers, is given by:

$$(8M + 8N) \quad (1)$$

If these motors carry cargo at their respective rates, V_A and V_B, the time the cargo spends in transport, in seconds, is equal to:

$$(8M/V_A + 8N/V_B) \quad (2)$$

The intermediate velocity, V, of these motors, in nanometers/second, is given by:

$$(8M + 8N) / (8M/V_A + 8N/V_B) = (M + N) / (M/V_A + N/V_B) \quad (3)$$

The effect of the mole fraction of the motors of type A on the speed of the cargo can be integrated into the equation using:

$$n = (M/(M+N)) \quad (4)$$

The velocity equation can be rearranged using the mole fraction as:

$$V = (V_A V_B) /(nV_B + (1-n)V_A) \quad (5)$$

The mechanical competition model assumes that instead of sequential stepping by one motor or another, as in the alternating action model, the two types of kinesin are both generating a force on the cargo at the same time. Though both forms of kinesin are plus-ended motors, the slower motors exert a drag force on the fast motors attached to the same cargo resulting in an intermediate velocity. This model assumes that no motors unbind from the microtubule and that all of them walk at the same speed. Neglecting the negligible force of drag (femtoNewtons) the net force produced on the cargo is the sum of the forces of the motors simultaneously attached. If f_A and f_B are the forces exerted by motors type A and B then the force balance can be modeled as:

$$M f_A + N f_B = F_A + F_B = 0 \; pN \quad (6)$$

with M and N representing the number of motors exerting their respective forces. The forces of the individual motors can be modeled themselves as the product of their stall force (the maximum force generation) and the ratio of the cargo velocity and their own unloaded velocity such that:

$$F_A = F_{StallA} (1 - V/ V_A) \text{ and } F_B = F_{StallB}(1-V / V_B) \quad (7)$$

Substituting in for F_A and F_B, the force balance can be modeled as:

$$MF_{StallA}(1 - V/V_A) + NF_{StallB}(1 - V/V_B) = 0 \quad (8)$$

As with the alternating action model, the mole fraction of type *A* can be integrated into this equation using the mole fraction given by (4). The equation can also be further reduced by using:

$$\gamma = F_{StallA} / F_{StallB} \quad (9)$$

as a ratio of the stall forces. The velocity of the cargo can now be represented as:

$$V = V_A V_B (n\gamma + (1 - n))/(n\gamma V_B + (1\text{-}n)V_A) \quad (10)$$

The alternating action model and the mechanical competition model both model the *in vitro* movement of microtubules well for their specific motors, but they do not take into account the effects that multiple motors will have on the unbinding rates, net internal forces, and velocities of individual motors. Multiple motor experiments have demonstrated that when there is more than one motor bound to a microtubule the unbinding rates of the individual motors vary from their values as single motors (Rogers, 2009). The force-velocity curve of single motors is linear, but multiple motors results in a non-linear curve also suggesting that the unbinding rates are dependent upon the force applied (Klumpp, 2005).

The validity of these models can be tested experimentally using different combinations of motors in microtubule gliding assays. Mixing motors in specific mole ratios will provide some insight into how accurately the alternating action and mechanical competition models predict the velocity for different motors with different characteristics. The accuracy of the models may vary depending on family of kinesin motors combined, the differences in the processivity and velocities of the motors, and the forces that they generate and exert on each other. These experiments can also be done using various motor concentrations to determine whether or not the results scale through a wide range of surface motor densities.

In order to account for some of the assumptions of the alternating action and mechanical competition models, a theoretical "transition rate" model has been proposed that takes into account the effect of binding and unbinding of motors from the microtubule during the run length resulting in a changing number of motors during transport. As with the other models, the number of motors of each type that are bound to the microtubule define the transport properties, but the transition rate model allows for the dissociation of motors and thus a different number of motors attached at any given time (Klumpp, 2005). The transition rate model is limited in its application as a predictor of cargo velocity due to the lack of experimental data available on multi-motor systems. Nonetheless, the transition rate model makes predictions that have been experimentally verified and its basic tenets should definitely be taken into consideration in the mathematical modeling of systems of molecular motors if only qualitatively.

Chapter 2: Materials and Methods

In vitro gliding motility assays are used to determine the speed of cargo being transported by the molecular motors in each experiment. These assays allow for the observation and measurement of microtubules being transported by motors using a combination of florescence microscopy and video recording and tracking software.

Rhodamine labeled tubulin polymerizes into microtubules that can be viewed under green fluorescent light. They are created using a solution of BRB80 buffer (80 mM PIPES, 1 mM $MgCl_2$, 1 mM EGTA, pH 6.9), 32 μM tubulin, 4 mM $MgCl_2$, 1 mM guanosine triphosphate, and 5% dimethyl sulfoxide placed in a thirty-seven degrees Celsius water bath for thirty minutes. After removing the solution from the water bath it should be quickly (within one minute) diluted 50-fold into a room temperature solution of BRB80 and 20 μM paclitaxel, a mitotic inhibitor, to prevent catastrophe of the microtubules back into their tubulin subunits.

First, a flow cell is constructed by attaching a clean glass microscope slide to a cover slip using a strip of double sided tape that has been cut lengthwise into two pieces and placed lengthwise on the microscope slide leaving roughly 1 centimeter between the strips. A solution of BRB80 and 0.6 mg/mL casein is first flowed through to block the surface of the microscope slide with casein. The motors will bind irreversibly to the casein and stay bound in place during the motility gliding assay.

Five minutes after the surface blocking solution is passed the glass slide is prepared to have a solution of motors passed over it. This solution is composed of BRB80, 1 mM MgATP and 0.2 mg/mL casein combined with the chosen concentration of kinesin motors being used to perform the microtubule gliding assay.

After five to ten minutes of letting the motors land and bind to the casein surface, the motility solution (BRB80, 20 μM paciltaxel, 0.2 mg/mL casein, 1 mM MgATP, 20 mM D-

glucose, 0.02 mg/mL glucose oxidase, 0.008 mg/mL catalase, 0.5% 2-mercaptoethanol, and 30 nM of polymerized tubulin) is flown over the motors. The motility solution should be kept at room temperature and passed twice through a 30 gauge needle at a flow rate of ~100 μL/s to shear the microtubules down to a length of one to five micrometers.

The temperature at which the experiment takes place should be kept as constant as possible and recorded as the temperature affects the speed at which the motors carry cargo. Also, if multiple assays are being performed at the same time with a changing variable the order in which the flow cells are observed should be randomized to prevent any time-dependent variables from affecting the data.

The movement of the microtubules by the motors within the flow cell is now ready to be observed using fluorescence microscopy with a 100x lens in low viscosity immersion oil. This motion is viewed using a Genwac GW-902H camera that outputs its display on a computer monitor. The video is recorded and saved to a hard drive using *Capwiz*. Using *VirtualDub*, the video is converted to an .avi file extension so that it can be viewed using *ImageJ* software. The movement of the microtubules is tracked using the "MTrackJ" plugin in the *ImageJ* application. Every 100 frames (3.3 seconds) the position of the microtubule is documented. The velocity of the microtubules is calculated by dividing the distance the microtubule moved in each 100 frame interval. Pressing "measure tracks" in the "MTrackJ" plugin displays a list of the velocities in the far right column. The velocity of each mole fraction is calculated by taking the average of these velocities. Providing there are enough microtubule landing events that result in processive runs, typically around forty velocities are averaged together. The standard error of the mean is then calculated for each average velocity at a specific mole ratio.

Chapter 3: Results

3.1 Microtubule Gliding Motility Assays with Multiple Kinesin Motors

To study how motors interact cooperatively to carry cargo, motility assays with different kinesin motors were used to analyze how different mole ratios of the motors affect the intermediate cargo transport velocity. Though the motors can not be viewed directly, their effect on the microtubule will be indicative of how motors cooperatively work together to carry cargo *in vivo*.

In order to properly analyze the effect that kinesin motors with different cargo transport velocities have on each other in an *in vitro* motility assay it is important to understand how the experiment is designed. Mixing different molecular motors in specific proportions requires that the mole ratios of the motors attached to the surface of the flow cell are correct. This is a result of determining the total motor density on the surface as well as the motor densities of the individual motors chosen for the assay.

Calculating the motor density per unit area requires knowledge of the concentration of the individual motors and the weight of the dimeric kinesin molecule. Assuming that all of the motors stick to the surface and that the flow cell is roughly 100 μm thick, for each 1 μm^2 of surface area, the motors in the 50 μm thick volume above each side will stick to the surface. For instance, a 100 μg/mL stock kinesin motor concentration is divided by its 200 kD molecular weight resulting in a molar concentration of 0.5 μM. The surface motor density is estimated to be 50 μm^3 x 10^{-18} $m^3/\mu m^3$ x 10^3 L/m^3 x $.5x10^{-6}$ mol/L x $6.02x10^{23}$ molecules/mol = 15050 motors/μm^2. Since stock motor solution concentrations typically result in an incredibly high motor density, the solution could then be diluted 100 times so that there are 150 motors/μm^2. In order to properly mix two kinesin motors it is important that each solution results in the same

number of total motors per unit area, which is most cases requires that the experimenter calculate and dilute the solutions accordingly.

Once the motor solutions are diluted to their proper concentrations, they can be mixed volumetrically to give the desired mole ratios of the two motors. The mixed solutions can then be flowed into a flow cell for use in microtubule gliding assays. The data from the gliding assays can give insight into how different motors interact with each other in specific ratios.

In these experiments, microtubule gliding assays were performed combining mixtures of conventional Kinesin-1 drosophila melanogaster kinesin heavy chain (DmKHC) and Kinesin-2 motors. DmKHC is a plus-end directed (anterograde) homodimeric processive motor with a 14 amino acid long neck linker. The two Kinesin-2 motors used in the experiments were heterodimeric KIF3A/B and mutated $KIF3A_{\Delta DAL.}$ The concentration of total motors on the surface was decided upon experimentally. Landing rate assays were performed on different motor concentrations to determine which motor density would result in a sufficient number of microtubule landing events that would provide velocity data. These concentrations were then scaled up and down by a constant factor to ensure that similar results could be obtained.

The two motors were combined in multiple mole fractions varying from 0% to 100% DmKHC. The data from these experiments is graphed below along with the curves for the alternating action model and the mechanical competition model.

3.2 Results of KIF3A/B-FL Kinesin-2 Mixed with Kinesin-1

For these experiments microtubule gliding assays performed using varying mole fractions of mixtures of DmKHC and KIF3A/B Full Length motors with estimated total motor concentrations of 36, 180, and 900 motors/μm^2. Each increasing motor concentration is five

times greater than the concentration before it, providing data regarding the scalability of the velocity models.

KIF3A/B is a less processive, anterograde Kinesin-2 motor involved in intraflagellar transport. Unlike DmKHC, KIF3A/B has two different motor domains, A and B, thus classifying it as a heterodimeric motor. The effect of having two different motor domains on gliding velocity has been experimentally determined to be negligible for this motor. Chimeric motors KIF3A/A and KIF3B/B have been shown to have very similar gliding velocities as KIF3A/B (Muthkrishnan, 2009).

KIF3A/B has three additional amino acid its neck linker making it seventeen amino acids long compared to Kinesin-1's fourteen amino acid neck linker. As mentioned previously, mechanical tension is believed to be transmitted between the two motor heads through the neck linker. By thinking of the neck linker as a mechanical spring connecting the two motor heads, it is easy to imagine that an extended neck linker will result in less tension between the two motor domains while both heads are bound to the microtubule. The reduction in mechanical tension between the two heads results in smaller loads being applied to the motor heads. This decreased plus-ended force on the rear head lowers the motor head's binding affinity for ADP. This means there is a smaller chance of the motor entering the weak microtubule bound state, thus making it less likely to unbind (Uemura, 2003). The extension in the neck linker likely results in an altered coordination of the hydrolysis cycle between the two motor heads as compared to conventional Kinesin-1. Kinesin-1 has been experimentally shown to walk along a microtubule four times longer than KIF3A/B before dissociating, thus having four times greater processivity.

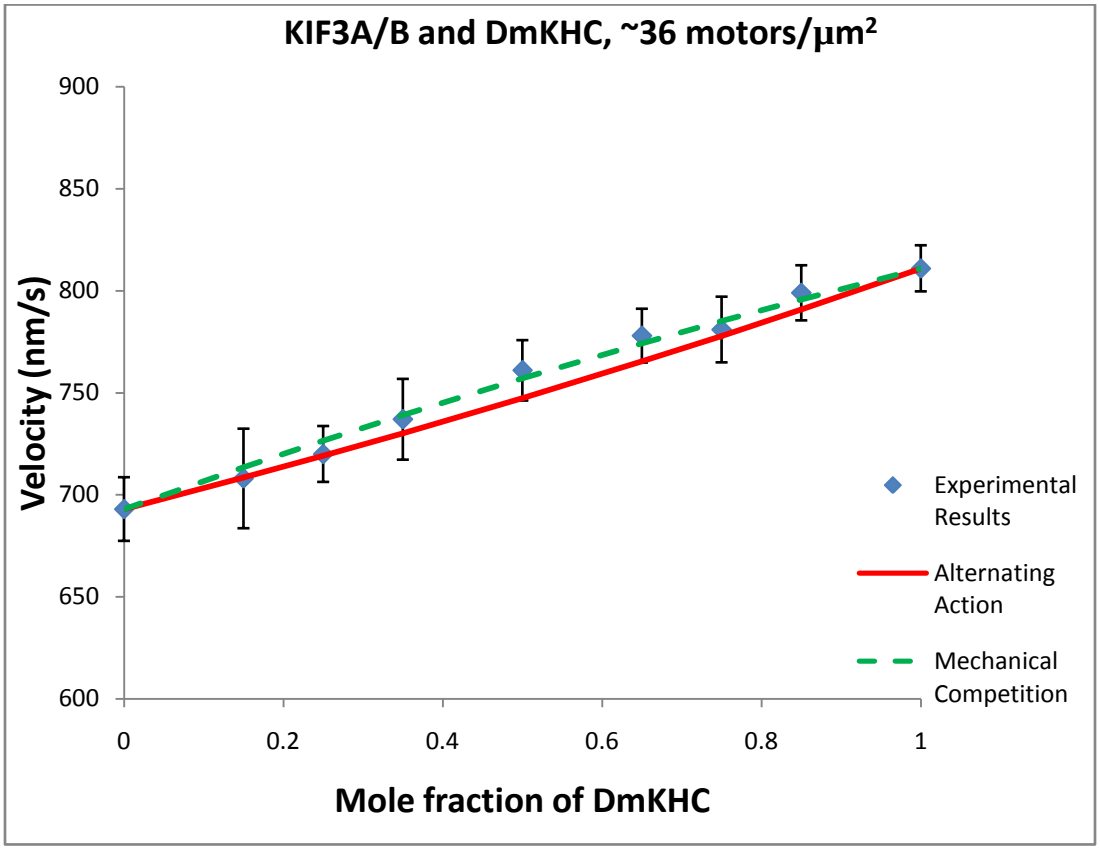

Figure 3-1: Velocity of microtubules in the microtubule gliding assay with different mole fractions of DmKHC motors mixed with KIF3A/B motors. An estimated total of 36 motors were bound to the surface per square micron. Experimental results are displayed with the standard error of the mean. Alternating action model: $\gamma = 1$, $R^2 = .984$. Mechanical competition model: $\gamma = 1.39$, $R^2 = .992$.

Figure 3-1 presents results of a microtubule gliding assay from a mixture of DmKHC and KIF3A/B with an estimated constant motor density of 36 motors per square micron. The velocity of the microtubules increases linearly from the first to the last point on the graph with the concentration of DmKHC varying from 0 to 100 percent. The coefficient of determination (R^2 value) comparing the alternating action model to the results is 0.984, strongly suggesting a linear relationship between the mole fraction of DmKHC in the solution and the velocity of the microtubules. Assuming that the ratio of the stall forces of the DmKHC and KIF3A/B are equal to 1, the mechanical competition model provides the same result. If the ratio of the stall forces is varied, the maximum coefficient of determination for the mechanical competition model

increases to 0.992 if the ratio of the stall forces equals 1.39, though the improvement in fit is rather negligible compared to the change in the stall forces.

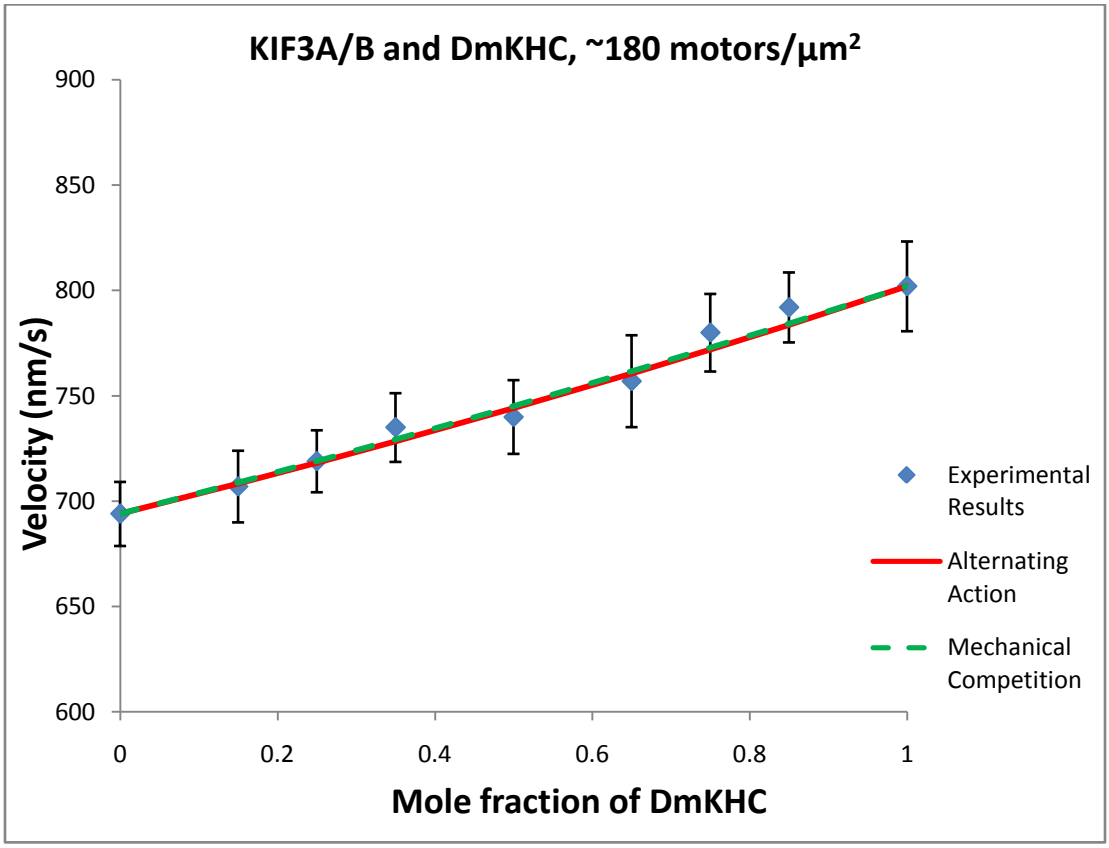

Figure 3-2: Velocity of microtubules in the microtubule gliding assay with different mole fractions of DmKHC motors mixed with KIF3A/B motors. An estimated total of 180 motors were bound to the surface per square micron. Experimental results are displayed with the standard error of the mean. Alternating action model: $\gamma = 1$, $R^2 = .980$. Mechanical competition model: $\gamma = 1.04$, $R^2 = .980$.

Figure 3-2 presents results of a microtubule gliding assay from a mixture of DmKHC and KIF3A/B with an estimated constant motor density of 180 motors per square micron. The trend of the velocities and the range of values are similar to the data from the mixture with 36 motors per square micron. The velocity of the microtubules again increases linearly across the range of mole fractions of DmKHC. The alternating action model's R^2 value strongly suggests that there is a linear relationship between the mole fraction of DmKHC and the velocity of the microtubules. The R^2 value of the mechanical competition model reaches its peak at a stall force

ratio very close to that of the alternating action model. As a result, the R^2 values of the two models differ by only a few ten-thousands.

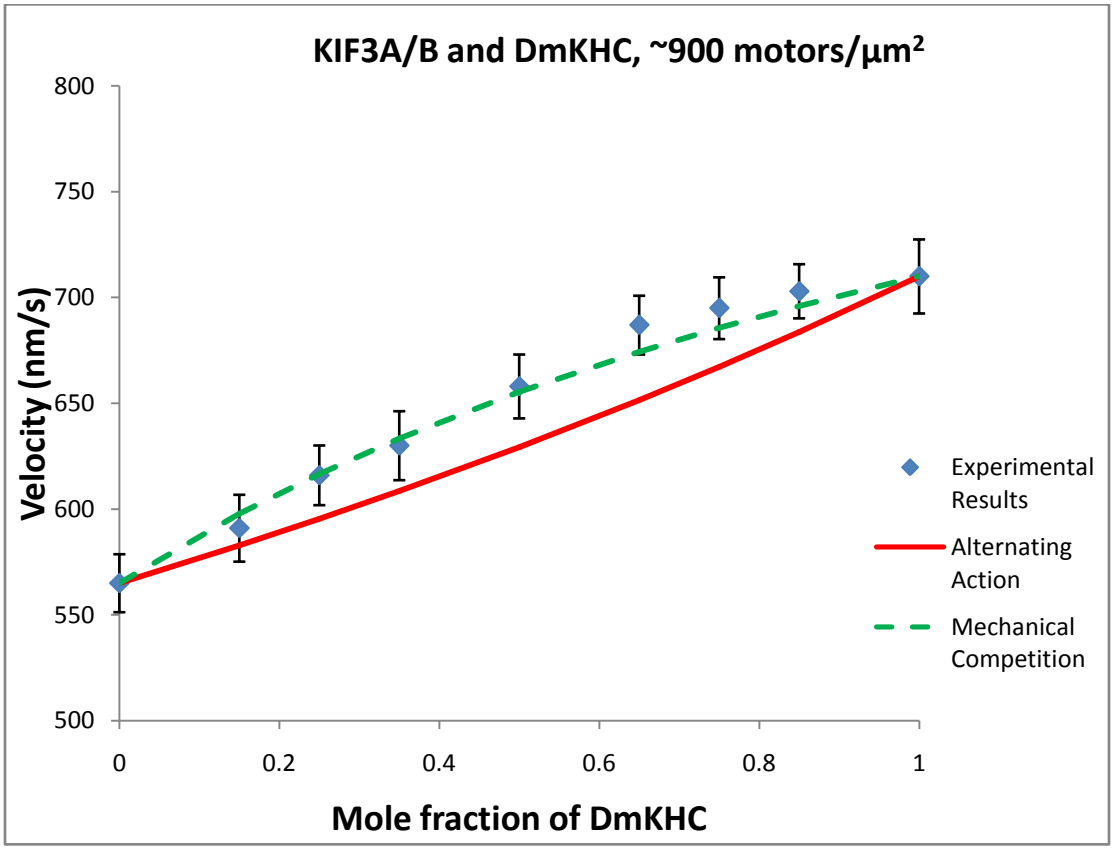

Figure 3-3: Velocity of microtubules in the microtubule gliding assay with different mole fractions of DmKHC motors mixed with KIF3A/B motors. An estimated total of 900 motors were bound to the surface per square micron. Experimental results are displayed with the standard error of the mean. Alternating action model: $\gamma = 1$, $R^2 = .944$. Mechanical competition model: $\gamma = 2.08$, $R^2 = .991$.

Figure 3-3 presents the results of a high motor density mixture of DmKHC and KIF3A/B that resemble the middle and low density gliding assays with a few differences. The range of velocity values from the low to the high end of the graph is similar, but the velocities themselves are somewhat lower. This may be a result of the high motor density having a greater number of dead motor heads that are slowing down the assay.

For this motility assay, the alternating action model fit did not fit quite as well as the middle and lower motor density assays as evidenced by the significantly lower R^2 value. The

mechanical competition model fits the experimental results much better if the ratio of the stall forces is increased to 2.08.

3.3 Results from KIF3A$_{\Delta DAL}$-KHC-FL Kinesin-2 mixed with Kinesin-1

Though alternating action model fit the data for the motility assays mixing DmKHC and KIF3A/B reasonably well, the validity of such a model for two processive motors is questionable because it is unlikely that either motor will dissociate from the microtubule during the run. By altering the ratio of the stall forces of DmKHC and KIF3A/B, the mechanical competition model gives a better fit for the data, but the ratios that give the best fit are not consistent between motor densities, varying by up to a factor of 2.

In the second set of experiments, KIF3A/B was replaced with KIF3A$_{\Delta DAL}$, another Kinesin-2 anterograde motor, and mixed with DmKHC. In the motor's name, the subscript "ΔDAL" refers to the three amino acid deletion from end the KIF3A neck-linker. This deletion shortens the neck linker from 17 amino acids to 14 amino acids like conventional Kinesin-1. The deletion of the three amino acids has been shown to have a very significant effect on the processivity of the motor. Instead of increasing the processivity by improving mechanical communication between the motor heads, the shortened neck linker results in a motor that is nonprocessive in single-motor assays due to its inability to reach the next microtubule binding site. KIF3A$_{\Delta DAL}$ has been experimentally determined to walk 10.8 ± 1.1 nm per interaction with a microtubule. Considering that kinesin motors take 8 nm steps, this motor very likely takes only one step per microtubule interaction before dissociating thus making it nonprocessive (Shastry, 2010).

Mixing a highly processive motor with a nonprocessive motor will likely give very different results than mixing two processive motors. The Kinesin-1 is expected to dominate the

assay because the nonprocessive $KIF3A_{\Delta DAL}$ will likely not stay bound to the microtubule like the KIF3A/B does. When mixed with KIF3A/B, the intermediate velocity of the cargo is relatively proportional to the mole fraction of DmKHC, but when mixed with $KIF3A_{\Delta DAL}$, the velocity is expected to rise sharply even at low mole fractions of DmKHC.

One thing to keep in mind when analyzing motility assay data is that at low motor concentrations of motors with low processivity very often there are only a few microtubules that land and process for long enough to get a sufficient amount of data. This can result in some missing data points and/or velocity points that do not fit the trend of the graph, especially when performing motility assays with a wide variety of different mole fractions.

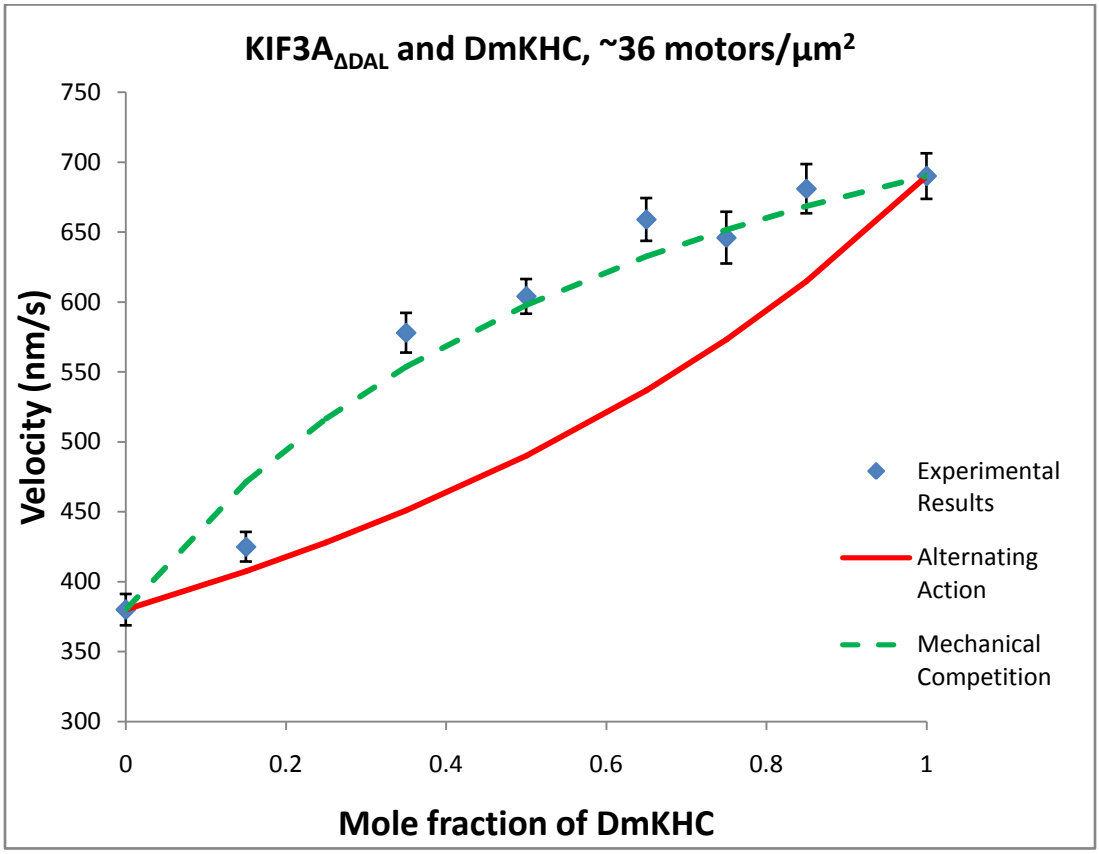

Figure 3-4: Velocity of microtubules in the microtubule gliding assay with different mole fractions of DmKHC motors mixed with KIF3A$_{\Delta DAL}$ motors. An estimated total of 36 motors were bound to the surface per square micron. Experimental results are displayed with the standard error of the mean. Alternating action model: $\gamma = 1$, $R^2 = .792$. Mechanical competition model: $\gamma = 4.30$, $R^2 = .968$.

Figure 3-4 presents the results of a low motor density mixture of DmKHC and KIF3A$_{\Delta DAL}$ with an estimated 36 motors per square micron. Though the velocity constantly increases from low DmKHC mole fractions to high mole fractions, the data is not quite as linear as the data from the KIF3A/B. When the mole ratio of DmKHC is increased from 0 to 0.5 the increase in velocity is more than double than the increase in velocity when the mole ratio is increased from 0.5 to 1. This suggests that a small mole fraction of DmKHC has a significant effect on the velocity of the microtubules in a mixture with KIF3A$_{\Delta DAL}$. In this experiment, the alternating action model fit the experimental values very poorly compared to the data using

KIF3A/B for a similar motor density. To maximize the R^2 value of the mechanical competition model the ratio of the stall forces needs to be increased over four-fold.

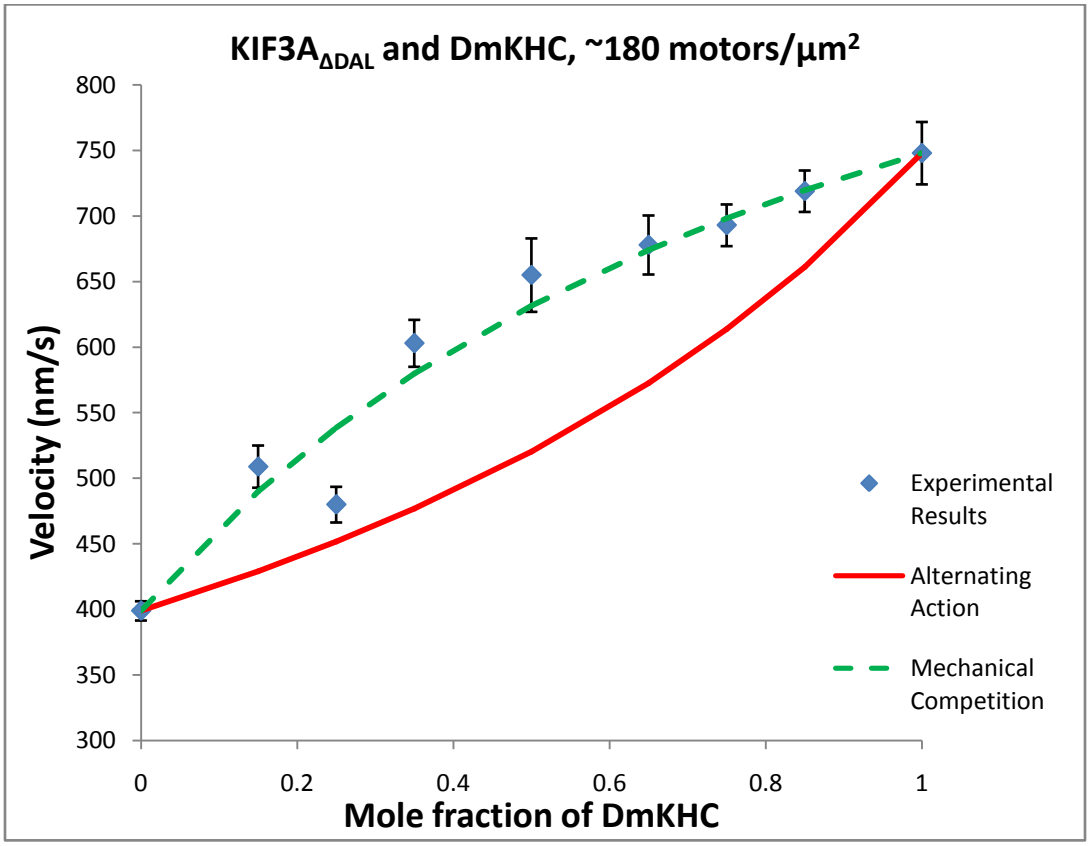

Figure 3-5: Velocity of microtubules in the microtubule gliding assay with different mole fractions of DmKHC motors mixed with KIF3A$_{\Delta DAL}$ motors. An estimated total of 180 motors were bound to the surface per square micron. Experimental results are displayed with the standard error of the mean. Alternating action model: $\gamma = 1$, $R^2 = .828$. Mechanical competition model: $\gamma = 3.75$, $R^2 = .958$.

When DmKHC and KIF3A$_{\Delta DAL}$ are mixed together in a motility assay with an estimated motor density of 180 motors per square micron the velocity increases in a slightly more linear trend than with the five-fold lower motor density, seen in Figure 3-5. When the mole ratio of DmKHC is increased from 0 to 0.5 the increase in velocity is over two and a half times greater than the increase in velocity when the mole ratio is increased from 0.5 to 1. Again, this suggests that a small proportion of DmKHC in this assay has a significant effect on the microtubule gliding velocity. The alternating action model fits slightly better in this assay than with the lower

motor density, though it is still quite low compared to the data from the KIF3A/B assay at a similar surface density. Like the low motor density assay, the ratio of the stall forces must be near four to maximize the coefficient of determination for the mechanical competition model fit.

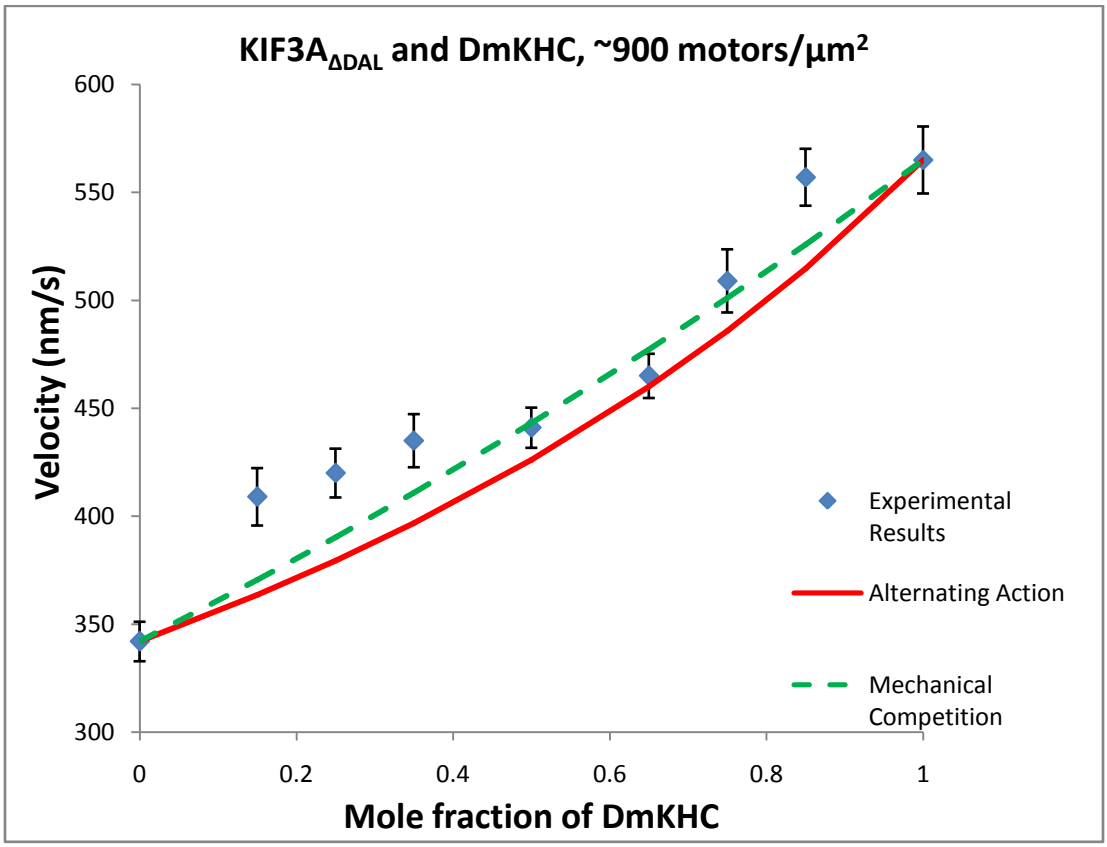

Figure 3-6: Velocity of microtubules in the microtubule gliding assay with different mole fractions of DmKHC motors mixed with KIF3A$_{\Delta DAL}$-KHC-FL motors. An estimated total of 900 motors were bound to the surface per square micron. Experimental results are displayed with the standard error of the mean. Alternating action model: $\gamma = 1$, $R^2 = .936$. Mechanical competition model: $\gamma = 1.37$, $R^2 = .943$.

The high motor density assay with approximately 900 motors per square micron, seen in Figure 3-6, had the most linear results of the three assays using DmKHC and KIF3A$_{\Delta DAL}$. The range of values for the assay is not quite as wide as in the other two experiments. Again, this may be the result of a greater number of dead motors heads bound to the microscope slide in the assay, slowing down the velocity. Compared to the lower motor density assays the alternating action

model fit the experimental data considerably better, almost exactly as well as the KIF3A/B assay with 900 motors per square micron. The mechanical competition model had a maximum R^2 value for a ratio of stall forces equal to 1.37, about 3 times lower than the ratio of stall forces needed for the other $KIF3A_{\Delta DAL}$ assays. The large decrease in the stall force ratio as the motor density increases may be the result of some other force parameter not being taken into account that becomes more significant as the motor density of the mixture increases.

3.4 Evaluation of the Mechanical Competition Model Using an Average Stall Force Ratio for KIF3A/B-FL Kinesin-2 Mixed with Kinesin-1

In Figures 3-1, 3-2, and 3-3 the stall force ratio used to calculate the mechanical competition model is varied for each motor density in order to get the highest coefficient of determination for each set of data. In reality, the stall force ratio of DmKHC and KIF3A/B should be held constant regardless of what the surface motor density is in the flow cell. To more rigorously assess the mechanical competition model the individual assay's stall force ratios are replaced by an average of the three ratios ($\gamma = 1.50$) for each motor density in Figures 3-7, 3-8, and 3-9 below. Using the average of the three stall force ratios evaluates the mechanical competition model more consistently across the range of motor densities than just selecting the stall force ratio with the best fit.

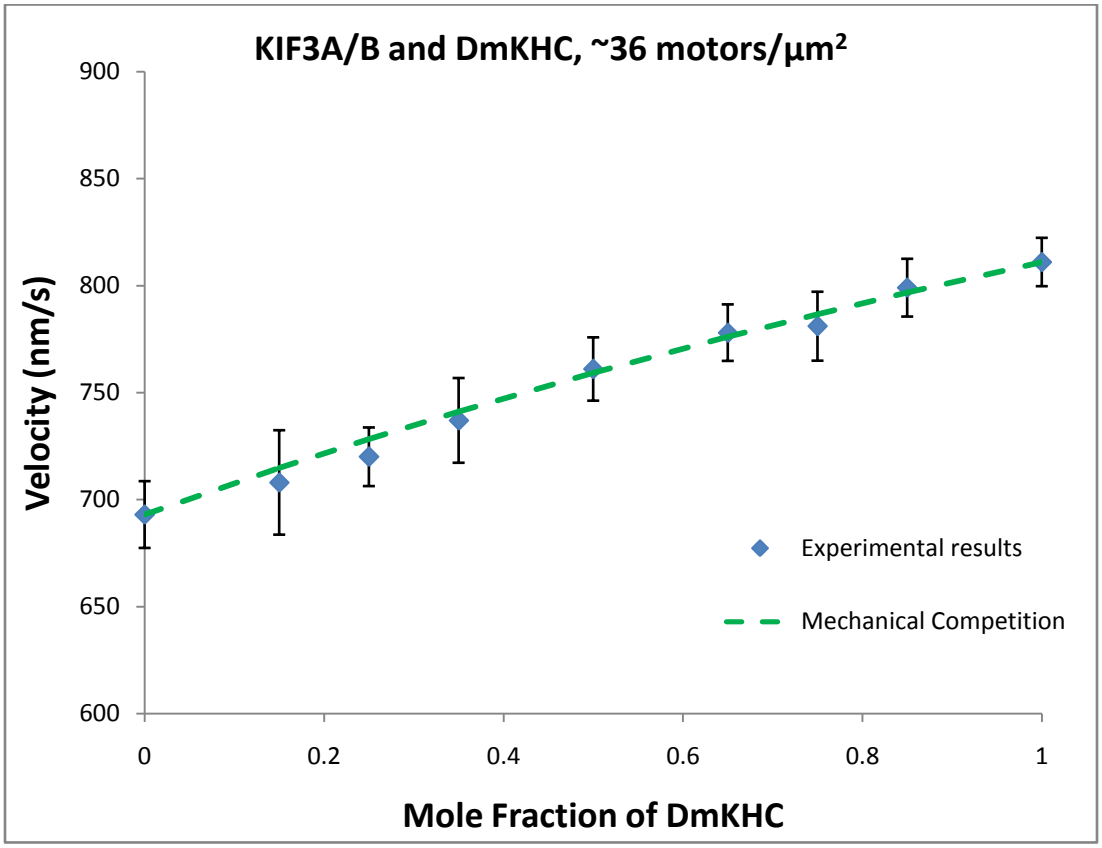

Figure 3-7: Velocity of microtubules in the microtubule gliding assay with different mole fractions of DmKHC motors mixed with KIF3A/B motors. An estimated total of 36 motors were bound to the surface per square micron. Experimental results are displayed with the standard error of the mean. Mechanical competition model: $\gamma = 1.50$, $R^2 = .992$.

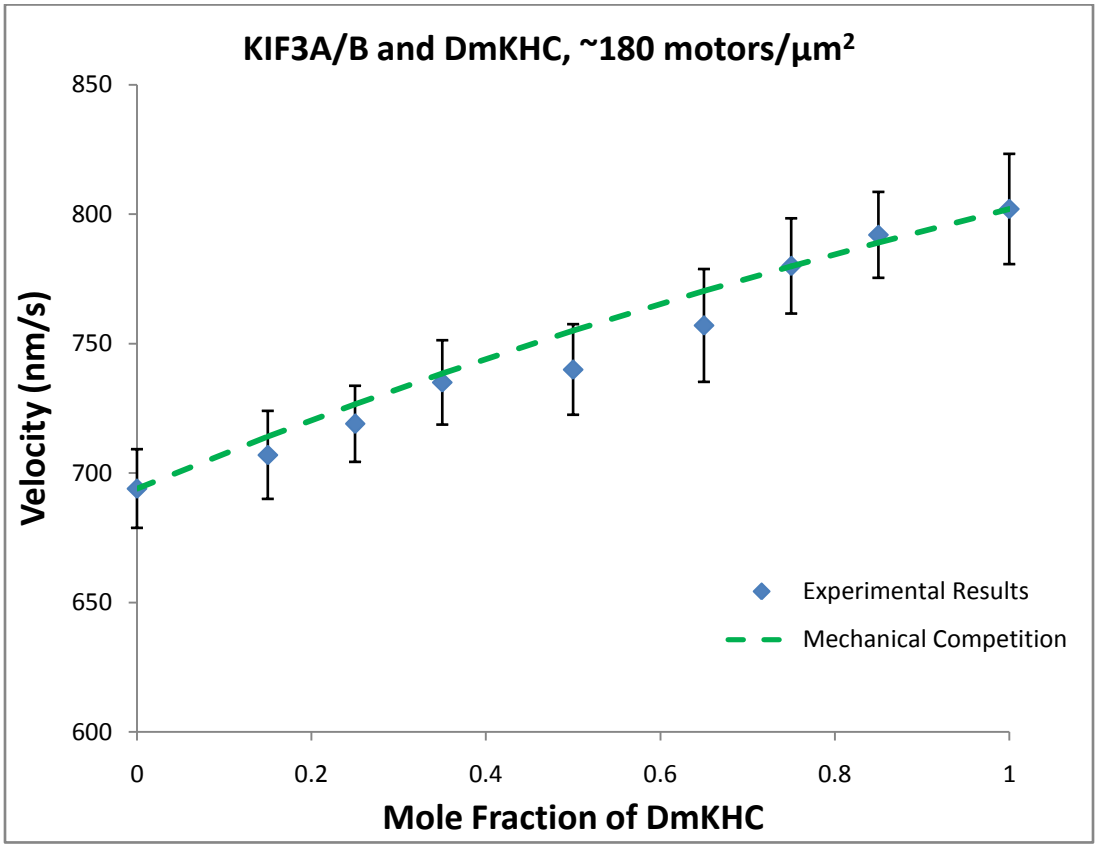

Figure 3-8: Velocity of microtubules in the microtubule gliding assay with different mole fractions of DmKHC motors mixed with KIF3A/B motors. An estimated total of 180 motors were bound to the surface per square micron. Experimental results are displayed with the standard error of the mean. Mechanical competition model: $\gamma = 1.50$, $R^2 = .973$.

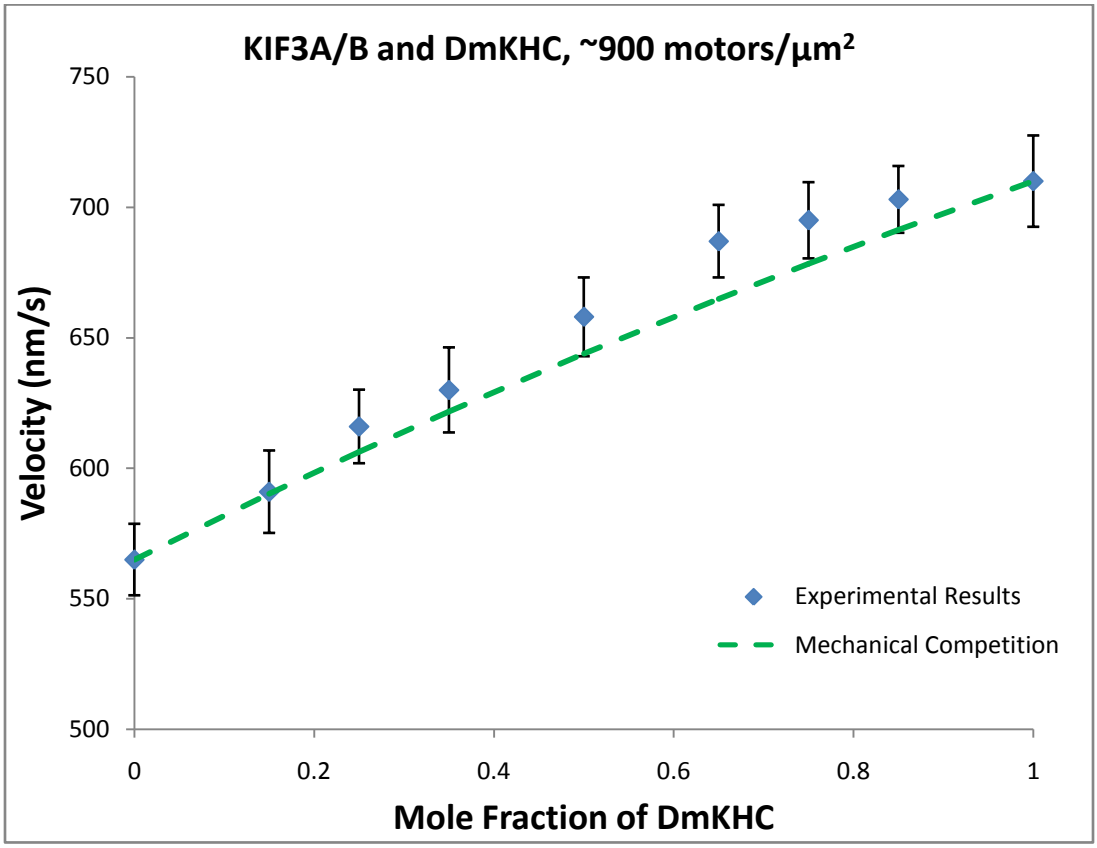

Figure 3-9: Velocity of microtubules in the microtubule gliding assay with different mole fractions of DmKHC motors mixed with KIF3A/B motors. An estimated total of 900 motors were bound to the surface per square micron. Experimental results are displayed with the standard error of the mean. Mechanical competition model: $\gamma = 1.50$, $R^2 = .981$.

When the stall force ratios used in the mechanical competition model are determined ad hoc by their best fit the coefficients of determination are very high for all three motor densities indicating that the model is accurate when the stall force ratio is a free parameter. When the three individual stall force ratios are averaged together and the mechanical competition model is recalculated for each set of experimental data the R^2 values are all also very high and near the original values, albeit slightly lower. This suggests that for mixtures of DmKHC and KIF3A/B the mechanical competition model fits the experimental data well regardless of the motor density in the flow cell.

3.5 Evaluation of the Mechanical Competition Model Using an Average Stall Force Ratio for KIF3A$_{\Delta DAL}$-KHC-FL Kinesin-2 Mixed with Kinesin-1

When the mechanical competition model is applied to mixtures of DmKHC and KIF3A$_{\Delta DAL}$-KHC-FL in Figures 3-4, 3-5, and 3-6 the stall force ratio is chosen to be the value that results in the highest coefficient of determination. As with the KIF3A/B motor, the ratio of the stall forces of DmKHC and KIF3A$_{\Delta DAL}$-KHC-FL should be a constant regardless of the motor density in the flow cell. In Figures 3-10, 3-11, and 3-12 the mechanical competition model is recalculated using an average of the three individual stall force ratios ($\gamma = 3.14$) and plotted against the original experimental results.

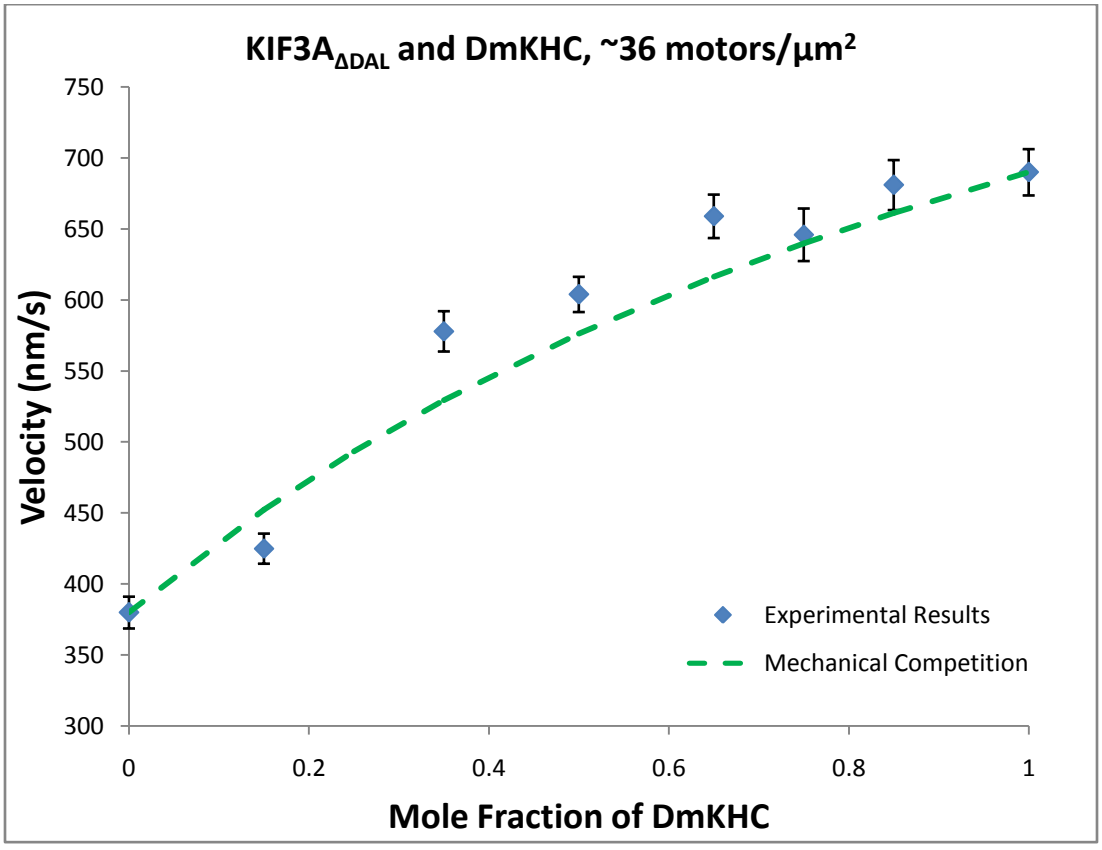

Figure 3-10: Velocity of microtubules in the microtubule gliding assay with different mole fractions of DmKHC motors mixed with KIF3A$_{\Delta DAL}$-KHC-FL motors. An estimated total of 36 motors were bound to the surface per square micron. Experimental results are displayed with the standard error of the mean. Mechanical competition model: $\gamma = 3.14$, $R^2 = .959$.

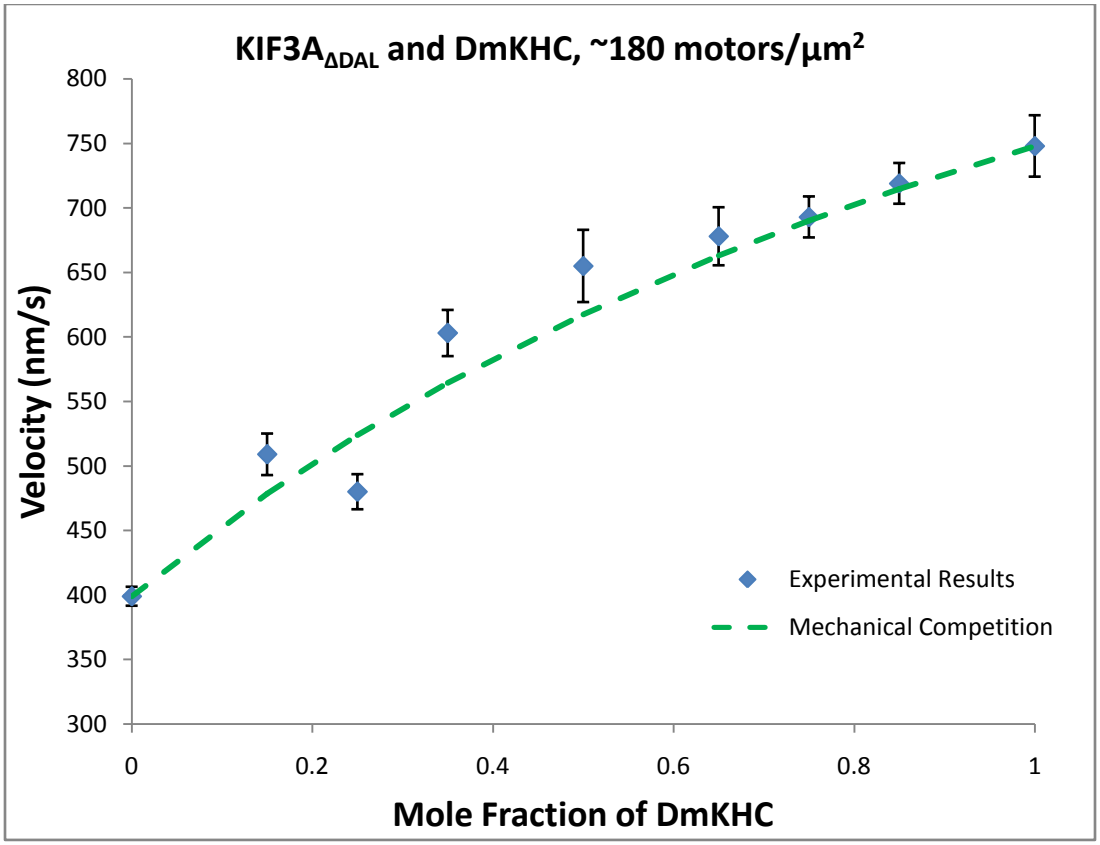

Figure 3-11: Velocity of microtubules in the microtubule gliding assay with different mole fractions of DmKHC motors mixed with KIF3A$_{\Delta DAL}$-KHC-FL motors. An estimated total of 180 motors were bound to the surface per square micron. Experimental results are displayed with the standard error of the mean. Mechanical competition model: $\gamma = 3.14$, $R^2 = .955$.

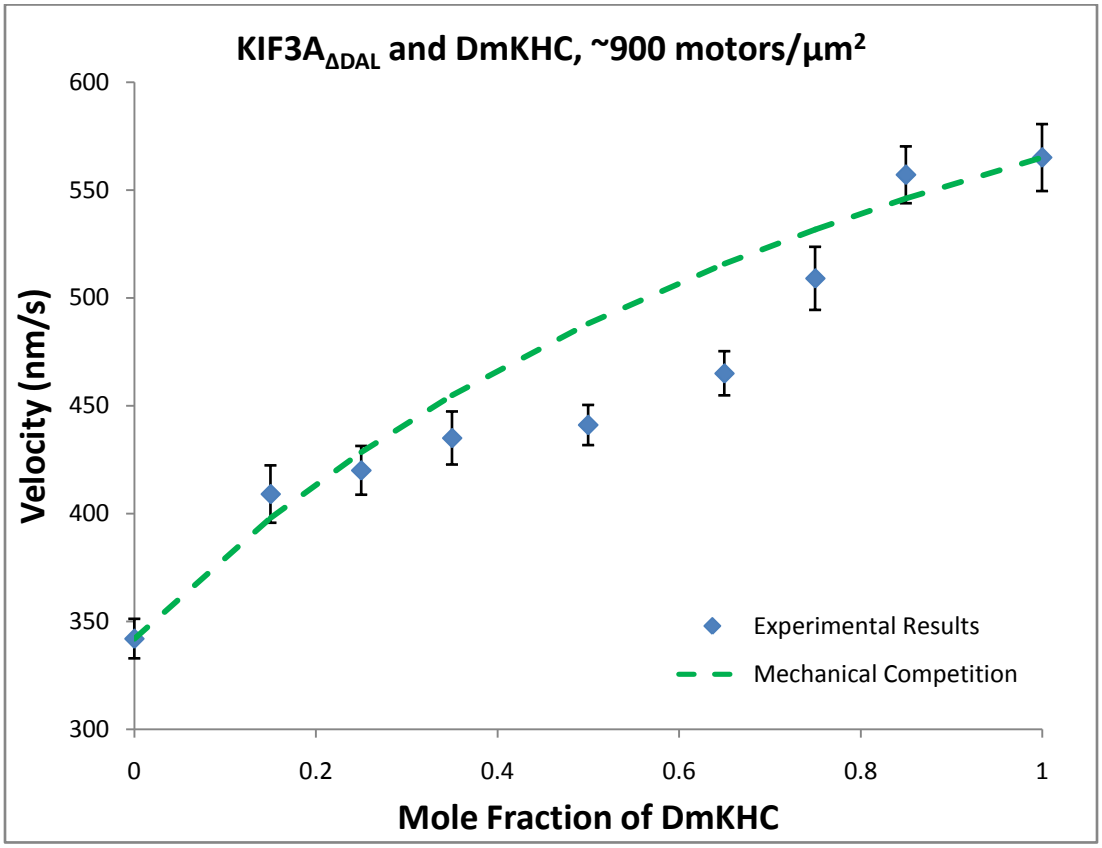

Figure 3-12: Velocity of microtubules in the microtubule gliding assay with different mole fractions of DmKHC motors mixed with KIF3A$_{\Delta DAL}$-KHC-FL motors. An estimated total of 900 motors were bound to the surface per square micron. Experimental results are displayed with the standard error of the mean. Mechanical competition model: $\gamma = 3.14$, $R^2 = .905$.

As with the KIF3A/B mixtures, the coefficient of determination is understandably lower when the stall force ratio is held constant at the average than if it is optimized for the best data fit. The decrease is only slight for the low and medium motor densities, but is more significant when the motor density is high. This is a result of the stall force ratio of the highest motor density mixture being significantly lower than the average value of all three stall force ratios implying that there is some unaccounted for parameter that becomes more significant as the motor density of the KIF3A$_{\Delta DAL}$-KHC-FL mixture increases.

Chapter 4: Discussion

4.1: Evaluation of Models

The goal of the experiments was to determine how accurate the alternating action and mechanical competition models are for modeling the effects of multiple kinesin motors on cargo transport velocity and under which circumstances they are most applicable. Microtubule motility gliding assays with different combinations of motors provides the proper method for performing such analysis. Mixing two motors in incremental mole ratios across different surface motor densities offers some insight into how kinesins cooperate when they are bound to the same cargo. Conventional Kinesin-1 mixed with Kinesin-2 motors with different speeds and processivities provides some data regarding how motors with dissimilar characteristics affect the cooperative transport of cargo.

The alternating action model and the mechanical competition model are good starting points for analyzing the data, but the transition rate model also provides insight into how the motors interact with each other. Unfortunately, it requires too many specific experimentally determined values for the variables to apply to the data here, but its implications are worth understanding.

In the transition rate model, average values for the bound number of motors of each type are calculated by using an iterative process until the results are within the desired tolerance. First, an estimation of the number of fast and slow bound motors, n_f and n_s, respectively, can be used to calculate the forces that each type of motor exerts on the microtubule as a function of the microtubule velocity and the individual velocities and stall forces of the motors:

$$F_+ = \left(1 - \frac{V_{mt}}{V_f}\right) n_f F_{\text{stall}}, \; F_- = \left(1 - \frac{V_{mt}}{V_s}\right) n_s F_{\text{stall}} \tag{11}$$

As mentioned before, the fast motors will produce a plus-ended force on the microtubule, while the slow motors exert a dragging minus-ended force. The collective force that each type of motor produces is distributed among the number of bound motors of the opposite type. These applied forces can be used to calculate the unbinding rates (ε). Assuming that the unbinding rate of the unloaded, individual motors (ε_0) and the motor dissociation force (F_d) are the same between the two different motors, the unbinding rate for each type of motor can be calculated from the estimated number of motors bound (n_f and n_s) and the collective directional forces applied (F_- and F_+) using (12). Additionally, the ratio of the asymmetrical dissociation forces, η, is accounted for in the calculation of the unbinding rate of the slow motors in (12), where $\eta \approx .45$:

$$\varepsilon_{n_f} = \varepsilon_0 n_f \exp\left[\frac{F_-}{n_f F_d}\right], \ \varepsilon_{n_s} = \varepsilon_0 n_s \exp\left[\frac{F_+}{n_s F_d \eta}\right] \tag{12}$$

The binding rates for assemblies of fast and slow motors can be calculated using (13) with the estimated maximum available number of motors to bind (N_f and N_s), the estimated number of motors bound (n_f and n_s), and the binding rate of the unloaded, individual motors, assuming that the last variable is equal between the two motors:

$$\pi_{nf} = (N_f - n_f)\pi_0, \ \pi_{ns} = (N_s - n_s)\pi_0 \tag{13}$$

Once these rates are determined, they can be used to calculate a motor binding probability distribution using (14):

$$P_{n_f} = \frac{\prod_{i=0}^{n_f-1} \frac{\pi_{n_f}}{\varepsilon_{n_f+1}}}{1 + \sum_{n_f=0}^{N_f-1} \prod_{i=0}^{n_f} \frac{\pi_{n_f}}{\varepsilon_{n_f+1}}}, \ P_{n_s} = \frac{\prod_{i=0}^{n_s-1} \frac{\pi_{n_s}}{\varepsilon_{n_s+1}}}{1 + \sum_{n_s=0}^{N_s-1} \prod_{i=0}^{n_s} \frac{\pi_{n_s}}{\varepsilon_{n_s+1}}} \tag{14}$$

From this probability binding distribution, the estimated number of bound motors is recalculated using (15):

$$\langle n_f \rangle = \sum_{n_f=1}^{N_f} n_f P_{n_f}, \ \langle n_s \rangle = \sum_{n_s=1}^{N_s} n_s P_{n_s} \tag{15}$$

The new number of bound motors is then used to subsequently recalculate the plus and minus-ended directed forces, unbinding and binding rates, and binding probability distributions. This iterative process is repeated for each mole fraction in the assay until the motor binding probability distributions are stable to within a 1% tolerance. When number of motors bound has been determined, the velocity of the microtubule can be calculated using the mechanical competition velocity formula as seen above. (Larson, 2009)

This model has been applied to sets of motors that have a wide difference in velocities. Figure 4-1 presents the results of a study where there were five point mutations made in the neck linker of a processive motor that resulted in a fifteen-fold decrease in speed. The study assumes that the other single molecule properties of the mutated motor do not vary from the single molecule properties of the original motor. Though, the model seems to predict the velocity very well, the assumption that the motor processivity, forces, and binding and unbinding rates stay constant despite all of the mutations is suspect considering how sensitive the neck linker has proven to be to changes in its composition.

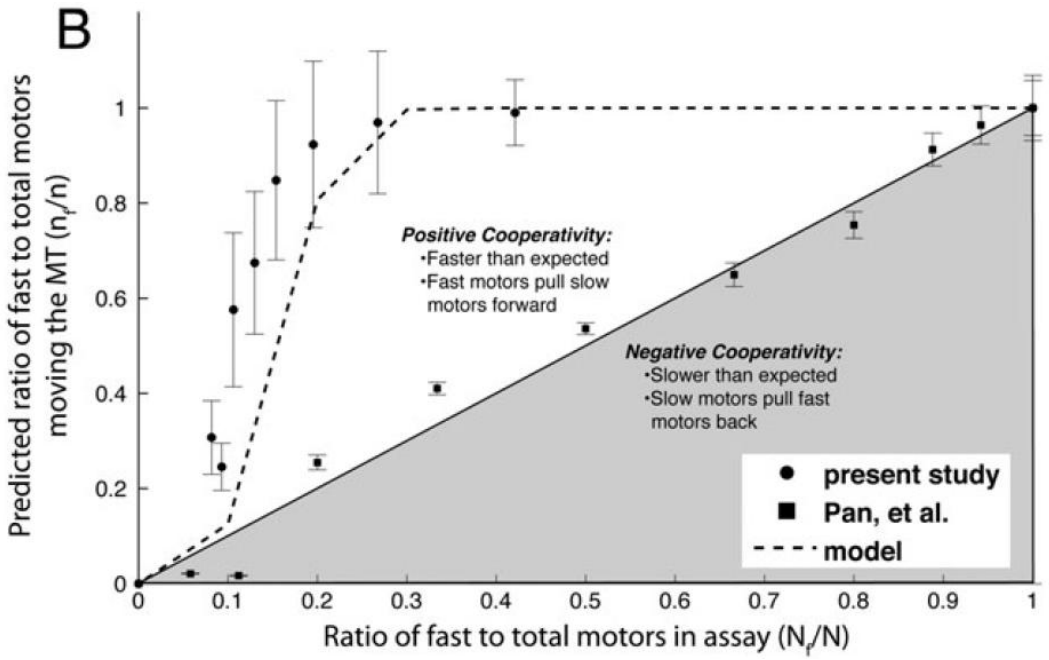

Figure 4-1: Velocity results of gliding assay of two motors with a fifteen fold difference in speed compared to the predicted results of the Pan et al. and transition rate models (Larson, 2009)

As mentioned previously, evidence suggests that when multiple kinesin motors are attached to a piece of cargo stepping is not necessarily synchronized. Internal forces on the microtubule are created by this uncoordinated stepping and are distributed across the bound motors, altering their unbinding rates. It is for this reason that the implications of the transition rate model should be taken into consideration even if specific values are not available for the variables.

The alternating action model generally resulted in very good modeling for the mixtures of DmKHC and KIF3A/B, especially when the motor concentrations were 36 and 180 motors per square micron, resulting in very high R^2 values. When the motor density in the flow cell is increased to 900 motors per square micron the coefficient of determination for the alternating action model drops slightly suggesting the influence of other elements on the velocity of the cargo.

When employing the mechanical competition model with the ratio of the stall forces set as a free parameter the fit of the data improves across all motor densities, albeit only slightly. The individual values for the ratio of the stall forces are not consistent across the motor densities and follow no clear trend. Seeing as how the alternating action model fits so well, it is reasonable to assume that the main factor in determining the intermediate cargo velocity of a mixture of DmKHC and KIF3A/B is the individual velocities of the motors. The velocity term may seem to be so significant because the individual velocities of the motors are very close, not providing much opportunity for other elements to noticeably influence the intermediate velocity.

When the individually determined stall forces are averaged together and plugged into the mechanical competition model the fit to the experimental data is better and more consistent than the alternating action model. This suggests that while velocity may be the most significant factor in determining the intermediate cargo velocity including the stall force term can have a positive effect on the model.

When DmKHC is mixed with KIF3A$_{\Delta DAL}$ the alternating action model does not predict the intermediate cargo transport velocity data nearly as well as it does for the KIF3A/B assays with low and medium motor density assays, as evidenced by Figures 3-4 and 3-5 and their respective coefficients of determination. Looking at the graphs, it is obvious that when DmKHC is in the mixture the intermediate velocity rapidly rises. When the DmKHC mole fraction is at 0.5, the increase in the velocity is nearly 73% of the total increase in velocity for both of the assays. The poor fit of the alternating action model at the lower densities suggests that even though individual motor velocity plays a large role in the intermediate transport velocity there are still significant factors missing from the model.

When the mechanical competition model is applied with high stall force ratios, the fit of the model to the experimental data was greatly improved. The vast improvement in fit indicates

that the ratio of the stall forces plays a significant role in the intermediate velocity data for these densities. When there are an estimated 900 motors per square micron the alternating action and mechanical competition models have very similar R^2 values, suggesting that the stall force ratio plays a smaller role in determining cargo velocity than in the lower motor densities.

When the mechanical competition model is recalculated using the average of the three individual stall force values it fits the two lower density assays fit much better than the alternating action model does, suggesting the importance of including the stall force ratio term. Though much improved, the mechanical competition model does not match the experimental data for this motor mixture as well as it does for the KIF3A/B mixtures. It is very likely that there are more significant transition rate elements that are not being taken into account in this case than with the previous mixtures.

On the other hand, when the recalculation is done for the high mote density assay it does not fit the data as well as the alternating action model. This discrepancy occurs because the best fit stall force ratio for the high density assay is significantly lower than other two thus making it farther from the average value. This decrease in fit is likely due to a change in the relative significance of velocity, stall force ratio, and transition rate elements with respect to the intermediate cargo velocity as the motor density increases.

These unaccounted for parameters may have a very significant influence on the transport velocity resulting in inaccurate stall force ratios. Without experimentally determined values of the stall forces of the motors, the ratio of the stall forces can not be concluded decisively. For example, the results from the experiments presented here unanimously suggest that Kinesin-1 can generate more force than Kinesin-2, implying that the former has the higher stall force of the two. Although each data set fit the mechanical competition model better when the stall force ratio of

Kinesin-1 to Kinesin-2 was greater than 1, the ratio is not consistent between the different motor densities indicating the presence of other elements that affect the cargo transport velocity.

Experimental data regarding the individual stall forces of Kinesin-1 and Kinesin-2 is not conclusive. Unpublished data from the Hancock and Block laboratories suggests that Kinesin-2 has a higher stall force than Kinesin-1. Their data indicates that the velocity of Kinesin-2 motors decrease more gradually than the velocity of Kinesin-1 motors when an increasing load is applied in the direction opposite of motion. This means that the force exerted by Kinesin-2 against the load is higher than the force exerted by Kinesin-1 thus implying that Kinesin-2 has a higher stall force ratio.

Other data suggests that the opposite is true regarding the stall forces of Kinesin-1 and Kinesin-2. When anterograde kinesin motors and retrograde dynein motors bind to the same microtubule a stochastic "tug of war" ensues that determines the movement of the microtubule depending on the strength and number of the motors working in both directions. Experimental data suggests that a 7:1 ratio of bound dynein motors to bound Kinesin-1 motors results in a directional force balance. The ratio of bound motors using dynein and Kinesin-2 in the experiment was found to be 3:2 (Hendricks, 2010). The data suggests that Kinesin-1 has a higher stall force than Kinesin-2 due to its ability to balance out the forces of more dynein motors than Kinesin-2.

Overall, the data suggests alternating action model is more accurate when KIF3A/B is mixed with DmKHC rather than $KIF3A_{\Delta DAL}$, especially for lower motor densities. The mechanical competition model improves the fit to the data due to having the ratio of the stall forces as a free parameter, though the value is not consistent across all motor densities. Using the average of the individual stall force ratios almost always provides a better fit than the alternating action model by itself. When averaging the stall force ratios, the individual values should first be

evaluated to see if any of them are outliers due to the effects of unaccounted for parameters that become more significant at different motor densities.

It stands to reason that the models proposed by Pan et al. gave better results for the KIF3A/B mixtures than the $KIF3A_{\Delta DAL}$ mixtures. The difference in velocity between KIF3A/B and DmKHC is significantly smaller than the difference in velocity between $KIF3A_{\Delta DAL}$ and DmKHC, meaning that the former set of motors exert less force on each other when uncoordinated stepping causes loads on the microtubule. In general, the faster motor would likely exert a plus-ended accelerating force on the slower motor, which would, in turn, exert a minus-ended drag force on the fast motor. Due to the asymmetry of dissociation forces, the plus-ended force is more likely to cause the slower motor to unbind from the microtubule. This implies that the $KIF3A_{\Delta DAL}$ is more likely to be pulled off of the microtubule due to the force exerted by the DmKHC than the KIF3A/B motors are. This can result in a cascading unbinding effect of the slower motors because as the number of slow motors decreases the disparity between the plus-ended and minus-ended forces grow larger. This causes more slow motors to unbind due to the force from the faster motors, even at low mole fractions of fast motors.

Another possible reason that the $KIF3A_{\Delta DAL}$ mixtures resemble a transition rate model more than the KIF3A/B mixtures could be due to its lack of processivity. Even though KIF3A/B is four times less processive than DmKHC, $KIF3A_{\Delta DAL}$ is nonprocessive. This means that the binding and unbinding rates of $KIF3A_{\Delta DAL}$ are similar to each other and that the motors are much more likely to dissociate from the microtubule at any time during a mixed motor microtubule run. The mole ratios of the different motors that are bound and actively transporting the microtubule may or may not be representative of the mole ratios of the motors that are available to bind.

It is surprising that when mixing an optimally processive motor like Kinesin-1 with a nonprocessive motor like $KIF3A_{\Delta DAL}$ that the Kinesin-1 does not completely dominate the gliding

assay. Kinesin-1 has a documented run length of about 250 steps while KIF3A$_{\Delta DAL}$ takes roughly 1 step for every microtubule interaction (Shastry, 2010). This means that at any time there should be hundreds of more Kinesin-1 molecules bound to the cargo than KIF3A$_{\Delta DAL}$ motors suggesting that the increase in the velocity at low mole ratios of DmKHC should be much sharper than it is in the results.

One possible explanation for the lack of a sharp transition between low and high velocities is that the KIF3A$_{\Delta DAL}$ may be rebinding very rapidly throughout the run. Even though the motors may not be assisting in transporting the microtubule, they may be rebinding to the microtubule so fast that they are effectively slowing down the speed that the DmKHC can move the microtubules. This may be a result of the geometries of the microtubule gliding assay. Since the motors are irreversibly bound in place, they may always be within close reach of the microtubule and thus bind very quickly.

Additionally, the KIF3A$_{\Delta DAL}$ may be bound to the microtubule tighter than previously thought. The Kinesin-1 may not be able to exert enough force on the microtubule to cause the slow motors to dissociate from it. Rather, the KIF3A$_{\Delta DAL}$ motors may be staying bound to the microtubule causing the DmKHC to generate a lesser net force on the microtubule, moving it at a slower rate. Without specific dissociation force data for the motors, though, this is not possible to determine.

When the surface motor density for the DmKHC and KIF3A$_{\Delta DAL}$ is increased to 900 motors per square micron, surprisingly, the alternating action model is almost as predictive as it was for the KIF3A/B mixture at the same motor density. Considering that the alternating action's coefficients of determination were significantly lower and the ratio of the stall forces in the best fit mechanical competition model were much higher for the low and middle motor density assays it seems as though the data from this motor mixture does not scale to high motor densities either.

At higher motor densities, with more motors available to bind to the microtubules, the transition rate model may vary from the data more because at high loads the force-velocity curve may not be linear (Larson 2009). The non-linear force data is then used to calculate the unbinding rates that increase exponentially leading to a further increase in the error. It should be noted that because many of the variables in the transition rate model are difficult to experimentally determine, like binding and unbinding rates for multiple motors, or are typically not accepted and published for specific motors, such as dissociation forces, in some cases the transition rate model may not be as correct as the simpler models.

From the results acquired, the alternating action/mechanical competition model seems to be a decently accurate model if used in the right conditions. Providing that the difference in gliding velocity between the motors is rather small (within two-fold) and the force generation is the same, or the ratio of stall forces is known, the model seems to fit the data very well as long as the motor density is not too high.

When the motors used in the system do not have similar characteristics or have a number of small differences, the transition rate model can help to better understand how the motors cooperate with each other and coordinate their movements. This model is very complex and has a lot of variables to take into account, including a number that cannot be well defined even though experimentation, but it can be used as a tool when the assay requires a more intricate analysis that goes beyond the scope of the maximum motor speeds, stall forces, and mole ratios.

4.2 Future Work

In order to better characterize the models that are presented here, much more experimentation is needed. There is very likely not one single, simple model that will accurately model any mixture of kinesin motors with very different properties at various concentrations.

In the future, a motility assay that mixes motors that have nearly all identical properties with the exception of one characteristic that varies a great deal would be a good experiment to run. These motors would be used to test various aspects of the transition rate model. For instance, a mixed motor gliding assay would be performed combining a slow motor and a very fast motor with a speed at least five times greater than the slow motor while keeping the processivity and force generation as constant as possible. This could possibly result in a very sharp velocity transition between the low and the high speed motors that was not seen in the experiments presented here.

Another experiment that would be beneficial to perform would be a mixed motor motility assay with two motors that have similar speeds and forces, but much different run lengths. This would help characterize how differences in processivity play a role in the velocities. This could possibly be done by mixing Kinesin-1 and a Kinesin-1 motor with a small mutation that inhibits its processivity, but leaves the other properties relatively unchanged, something that would be determined experimentally. As mentioned in the discussion, it is expected that the nonprocessive motor would get completely dominated by a processive one because of its higher unbinding rate, but there is currently not enough direct evidence to support this claim. These experiments would also be carried out over a range of motor densities to determine the scalability of the data.

In general, it would be beneficial to obtain data for the properties of the individual motors used in the experiments. Though there is no data currently published regarding the stall force for Kinesin-2 motors, it would be helpful to know the exact value of the stall force when modeling how it transports cargo cooperatively with Kinesin-1. Additionally, the binding and unbinding rates for individual motors would improve accuracy of the transition rate model, especially if the force-velocity relationship is better understood for assemblies of multiple motors causing loads on the microtubule cargo. Though it would take a lot of supplementary experimentation to get

more accurate values for the properties of individual motors and motor assemblies, having the data could be invaluable to understanding the cooperation between two specific motors. Ideally, these experiments would be performed on the exact motors used in the motility gliding assay experiments because there may be variations in properties between different protein preparations.

More extensive and varied experimentation would be necessary to better understand what conditions are the most appropriate to use the alternating action, mechanical competition, and/or transition rate models to model velocity of multiple kinesin motor gliding assays. The scope of the experiments presented here is very small compared the analysis that could be done on systems of multiple motors.

References

Asbury, C. (2005). "Kinesin: world's tiniest biped." Current opinion in cell biology 17(1): 89-97.

Asenjo, A., Y. Weinberg and H. Sosa (2006). "Nucleotide binding and hydrolysis induces a disorder-order transition in the kinesin neck-linker region." Nature Structural & Molecular Biology 13(7): 648-654.

Ashkin, A., K. Schtze, J. M. Dziedzic, U. Euteneuer and M. Schliwa (1990). "Force generation of organelle transport measured in vivo by an infrared laser trap." Nature 348(6299): 346-348.

Bieling, P., I. Telley, J. Piehler and T. Surrey (2008). "Processive kinesins require loose mechanical coupling for efficient collective motility." EMBO Reports 9(11): 1121-1127.

Bloom, G. S., M. C. Wagner, K. K. Pfister and S. T. Brady (1988). "Native structure and physical properties of bovine brain kinesin and identification of the ATP-binding subunit polypeptide." Biochemistry 27(9): 3409-3416.

Case, R. B., S. Rice, C. L. Hart, B. Ly and R. D. Vale (2000). "Role of the kinesin neck linker and catalytic core in microtubule-based motility." Current biology 10(3): 157-160.

Coy, D. L., W. O. Hancock, M. Wagenbach and J. Howard (1999). "Kinesin's tail domain is an inhibitory regulator of the motor domain." Nature Cell Biology 1(5): 288-292.

Hancock, W. O. and J. Howard (1998). "Processivity of the motor protein kinesin requires two heads." The journal of cell biology 140(6): 1395-1405.

Hancock, W. O. and J. Howard (1999). "Kinesin's processivity results from mechanical and chemical coordination between the ATP hydrolysis cycles of the two motor domains." Proceedings of the National Academy of Sciences of the United States of America 96(23): 13147-13152.

Hendricks, Adam G.; Perison, Eran; Ross, Jennifer; Schroeder, Harry W.; Tokito, Mariko; Holzbaur, Erika (2010). "Motor Coordination via Tug-of-War Mechanism Drives Bidirectional Vesicle Transport." Current Biology 20(8): R697-R702.

Hirokawa, N., K. K. Pfister, H. Yorifuji, M. C. Wagner, S. T. Brady and G. S. Bloom (1989). "Submolecular domains of bovine brain kinesin identified by electron microscopy and monoclonal antibody decoration." Cell 56(5): 867-878.

Hua, W., J. Chung and J. Gelles (2002). "Distinguishing inchworm and hand-over-hand processive kinesin movement by neck rotation measurements." Science 295(5556): 844-848.

Kawaguchi, K. and S. Ishiwata (2001). "Nucleotide-dependent single- to double-headed binding of kinesin." Science 291(5504): 667-669.

Klumpp, S. and R. Lipowsky (2005). "Cooperative cargo transport by several molecular motors." Proceedings of the National Academy of Sciences of the United States of America 102(48): 17284-17289.

Kull, F. J., E. P. Sablin, R. Lau, R. J. Fletterick and R. D. Vale (1996). "Crystal structure of the kinesin motor domain reveals a structural similarity to myosin." Nature 380(6574): 550-555.

Kural, C., H. Kim, S. Syed, G. Goshima, V. Gelfand and P. Selvin (2005). "Kinesin and dynein move a peroxisome in vivo: a tug-of-war or coordinated movement?" Science 308(5727): 1469-1472.

Kuznetsov, S. A., G. M. Langford and D. G. Weiss (1992). "Actin-dependent organelle movement in squid axoplasm." Nature 356(6371): 722-725.

Larson, A., E. Landahl and S. Rice (2009). "Mechanism of cooperative behaviour in systems of slow and fast molecular motors." Physical chemistry chemical physics 11(24): 4890-4898.

Levi, V., A. Serpinskaya, E. Gratton and V. Gelfand (2006). "Organelle transport along microtubules in Xenopus melanophores: evidence for cooperation between multiple motors." Biophysical Journal 90(1): 318-327.

Li, H., D. DeRosier, W. Nicholson, E. Nogales and K. Downing (2002). "Microtubule structure at 8 A resolution." Structure 10(10): 1317-1328.

Mallik, R. and S. Gross (2004). "Molecular motors: strategies to get along." Current biology 14(22): R971-R982.

Mandelkow, E. and A. Hoenger (1999). "Structures of kinesin and kinesin-microtubule interactions." Current opinion in cell biology 11(1): 34-44.

Müller, M. J. I., S. Klumpp and R. Lipowsky (2008). "Tug-of-war as a cooperative mechanism for bidirectional cargo transport by molecular motors." Proceedings of the National Academy of Sciences of the United States of America 105(12): 4609-4614.

Muthukrishnan, G., Y. Zhang, S. Shastry and W. Hancock (2009). "The processivity of kinesin-2 motors suggests diminished front-head gating." Current biology 19(5): 442-447.

Ozeki, T., V. Verma, M. Uppalapati, Y. Suzuki, M. Nakamura, J. Catchmark and W. Hancock (2009). "Surface-bound casein modulates the adsorption and activity of kinesin on SiO2 surfaces." Biophysical Journal 96(8): 3305-3318.

Pan, X., G. Ou, G. Civelekoglu-Scholey, O. Blacque, N. Endres, L. Tao, A. Mogilner, M. Leroux, R. Vale and J. Scholey (2006). "Mechanism of transport of IFT particles in C. elegans cilia by the concerted action of kinesin-II and OSM-3 motors." The journal of cell biology 174(7): 1035-1045.

Rogers, A., J. Driver, P. Constantinou, D. K. Jamison and M. Diehl (2009). "Negative interference dominates collective transport of kinesin motors in the absence of load." Physical chemistry chemical physics 11(24): 4882-4889.

Rosenfeld, S., P. Fordyce, G. Jefferson, P. King and S. Block (2003). "Stepping and stretching. How kinesin uses internal strain to walk processively." The Journal of biological chemistry 278(20): 18550-18556.

Schiff, P. B., J. Fant and S. B. Horwitz (1979). "Promotion of microtubule assembly in vitro by taxol." Nature 277(5698): 665-667.

Schnitzer, M. J. and S. M. Block (1997). "Kinesin hydrolyses one ATP per 8-nm step." Nature 388(6640): 386-390.

Shastry, S., Hancock, William O. (2010). "Neck Linker Length Determines the Degree of Processivity in Kinesin-1 and Kinesin-2 Motors." Current Biology In Press.

Tilney, L. G., J. Bryan, D. J. Bush, K. Fujiwara, M. S. Mooseker, D. B. Murphy and D. H. Snyder (1973). "Microtubules: evidence for 13 protofilaments." The journal of cell biology 59(2): 267-275.

Toprak, E., A. Yildiz, M. Hoffman, S. Rosenfeld and P. Selvin (2009). "Why kinesin is so processive." Proceedings of the National Academy of Sciences of the United States of America 106(31): 12717-12722.

Uemura, S. and S. i. Ishiwata (2003). "Loading direction regulates the affinity of ADP for kinesin." Nature structural biology 10(4): 308-311.

Uemura, S., K. Kawaguchi, J. Yajima, M. Edamatsu, Y. Toyoshima and S. i. Ishiwata (2002). "Kinesin-microtubule binding depends on both nucleotide state and loading direction." Proceedings of the National Academy of Sciences of the United States of America 99(9): 5977-5981.

Vale, R. D., T. S. Reese and M. P. Sheetz (1985). "Identification of a novel force-generating protein, kinesin, involved in microtubule-based motility." Cell 42(1): 39-50.

Vershinin, M., B. Carter, D. Razafsky, S. King and S. Gross (2007). "Multiple-motor based transport and its regulation by Tau." Proceedings of the National Academy of Sciences of the United States of America 104(1): 87-92.

Yang, J. T., W. M. Saxton, R. J. Stewart, E. C. Raff and L. S. Goldstein (1990). "Evidence that the head of kinesin is sufficient for force generation and motility in vitro." Science 249(4964): 42-47.

Yildiz, A., M. Tomishige, R. Vale and P. Selvin (2004). "Kinesin walks hand-over-hand." Science 303(5658): 676-678.

Nicholas R. Bizzaro

524 Locust Lane
State College PA, 16801
(215)-896-6524
NRB5026@psu.edu

Education

The Pennsylvania State University, University Park, PA
The Schreyer Honors College
Expected Graduation Date - December 2010
Bachelor of Science in Bioengineering
Chemical Engineering option
Dean's List: All semesters since matriculation

Experience

Penn State Bioengineering Department **January 2009 – Present**
Undergraduate Researcher

- Investigate how combinations of different kinesin motors at various dilutions work cooperatively to transport cargo using *in vitro* motility assays and mathematical modeling
- Undergraduate honors thesis expected to be complete by December 2010 under the supervision of Dr. William O. Hancock, Ph.D.

Activities

Sigma Phi Epsilon Fraternity - President **November 2008- November 2009**

- Overviewed and managed all aspects of the ninety man fraternity chapter including finances, member recruitment and development, alumni relations, risk management, social events, philanthropies and community service projects

Mount Nittany Medical Center Volunteer **September 2008 – Present**

- Recorded over sixty hours performing a variety of tasks in the hospital including discharging patients, transporting medical equipment and delivering mail and meals to patients

Penn State Boxing Team **November 2007 – April 2008**

- Conditioned, sparred and practiced boxing technique over fifteen hours per week via four night and three morning practices in preparation for intercollegiate competitions

Honors and Awards

- Tau Beta Pi Engineering Honor Society
- William A. Schreyer Award for Academic Excellence (Spring 2007, Spring 2008)
- 2007 Interfraternity Council New Member of the Year